Accepted Manuscript

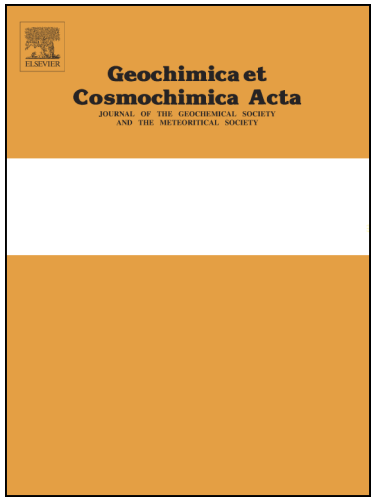

Integrating ^{40}Ar–^{39}Ar, ^{87}Rb–^{87}Sr and ^{147}Sm–^{143}Nd geochronology of authigenic illite to evaluate tectonic reactivation in an intraplate setting, central Australia

Alexander W. Middleton, I. Tonguç Uysal, Scott E. Bryan, Chris M. Hall, Suzanne D. Golding

PII: S0016-7037(14)00173-2
DOI: http://dx.doi.org/10.1016/j.gca.2014.02.048
Reference: GCA 8715

To appear in: *Geochimica et Cosmochimica Acta*

Received Date: 6 July 2013
Accepted Date: 24 February 2014

Please cite this article as: Middleton, A.W., Tonguç Uysal, I., Bryan, S.E., Hall, C.M., Golding, S.D., Integrating ^{40}Ar–^{39}Ar, ^{87}Rb–^{87}Sr and ^{147}Sm–^{143}Nd geochronology of authigenic illite to evaluate tectonic reactivation in an intraplate setting, central Australia, *Geochimica et Cosmochimica Acta* (2014), doi: http://dx.doi.org/10.1016/j.gca.2014.02.048

Integrating ^{40}Ar–^{39}Ar, ^{87}Rb–^{87}Sr and ^{147}Sm–^{143}Nd geochronology of authigenic illite to evaluate tectonic reactivation in an intraplate setting, central Australia

Alexander W. Middleton*[a], I. Tonguç Uysal [a], Scott E. Bryan[b], Chris M. Hall[c] and Suzanne D. Golding [d]

[a] *Queensland Geothermal Energy Centre of Excellence, The University of Queensland, Queensland 4072, Australia*

[b] *Biogeoscience, Queensland University of Technology, 1 George Street, Brisbane, QLD 4001, Australia*

[c] *Department of Earth and Environmental Sciences, University of Michigan, 1100 N. University Ave. Ann Arbor, MI 48109-1005, USA*

[d] *School of Earth Science, The University of Queensland, Queensland 4072, Australia*

Abstract

The Warburton–Cooper basins, central Australia, include a multitude of reactivated fracture–fault networks related to a complex, and poorly understood, tectonic evolution. We investigated authigenic illites from a granitic intrusion and sedimentary rocks associated with prominent structural features (Gidgealpa–Merrimelia–Innamincka Ridge and the Nappamerri Trough). These were analysed by ^{40}Ar–^{39}Ar, ^{87}Rb–^{87}Sr and ^{147}Sm–^{143}Nd geochronology to explore the thermal and tectonic histories of central Australian basins. The combined age data provide evidence for three major periods of fault reactivation throughout the Phanerozoic. While Carboniferous (323.3 ± 9.4 Ma) and Late Triassic ages (201.7 ± 9.3 Ma) derive from

basin-wide hydrothermal circulation, Cretaceous ages (~128 to ~86 Ma) reflect episodic fluid flow events restricted to the synclinal Nappamerri Trough. Such events result from regional extensional tectonism derived from the transferral of far-field stresses to mechanically and thermally weakened regions of the Australian continent. Specifically, Cretaceous ages reflect continent-wide transmission of tensional stress from a > 2500 km long rifting event on the Eastern (and southern) Australian margin associated with break-up of Gondwana and opening of the Tasman Sea. By integrating ^{40}Ar–^{39}Ar, ^{87}Rb–^{87}Sr and ^{147}Sm–^{143}Nd dating, this study highlights the use of authigenic illite in temporally constraining the tectonic evolution of intracontinental basins that would otherwise remain unknown. Furthermore, combining Sr- and Ar-isotopic systems enables more accurate dating of authigenesis whilst significantly reducing geochemical pitfalls commonly associated with these radioisotopic dating methods.

Corresponding author Tel: +61 422708045

Email Address: alexander.middleton@uqconnect.edu.au

Keywords: Fluid flow history, Warburton–Cooper Basin, ^{40}Ar–^{39}Ar geochronology, ^{87}Rb–^{87}Sr geochronology, illite.

1. INTRODUCTION

The central Australian Warburton–Cooper–Eromanga basins host one of the most prospective hot dry-rock geothermal resources in the world as well as significant

onshore hydrocarbon resources related to from unusually high palaeo- and current heat-flow (Deighton and Hill, 1998; APPEA, 2003; Hillis et al., 2004). To date, little is known about the timing and extent of palaeotectonism controlling the thermal history of these basins. This is largely due to the absence of any substantial outcrop and the presence of multiple unconformities that leave >180 Ma of basin history unrecorded. Recent investigations identified a network of reactivated normal–thrust fault systems attributed to several orogenic pulses, periods of uplift and plate-wide compressional stress (Apak et al., 1997; Mavromatidis, 2006; Rezaee and Sun, 2007). As such, this work highlights a potentially complex tectonic history atypical for most intracontinental sedimentary basins. This poses the question of, how and why does an area of central Australia, that should be tectonically quiescent due to its distance from plate boundaries, have an apparently convoluted tectonic and hence, thermal evolution? Currently, very few chronological constraints exist for the Warburton–Cooper basins (Gatehouse et al., 1995; Zwingmann et al., 2001; McLaren and Dunlap, 2006). These include U–Pb SHRIMP and ^{40}Ar–^{39}Ar of primary zircon and K-feldspar, respectively, from the highly altered, high heat-producing Big Lake Suite granite (Gatehouse et al., 1995; McLaren and Dunlap, 2006). However, previous studies have shown primary zircon and K-feldspar may experience alteration and recrystallisation under certain physico-chemical conditions in fluid-rich hydrothermal systems (Gerdes and Zeh, 2009; Nasdala et al., 2010). Therefore, it may not be possible to use these minerals to constrain the timing of regional tectonomagmatic activity (Cassata and Renne, 2013). In such cases, illitic clay minerals can offer a more robust alternative (Uysal et al., 2001; Golding et al., 2006; Uysal et al., 2006).

Illitic clays can precipitate as a result of fluid–rock interaction during migration of tectonically-driven fluids along permeable fracture networks. Owing to its composition it can be used for a suite of geochemical and geochronological analyses. As

illites contain particular radioactive elements (K, Rb and Sm), radiogenic isotope studies can determine the timing of fluid flow events associated with active tectonism. Moreover, if multiple generations of illite are identified, geochronology can determine episodic fluid flow and, therefore, reconstruct thermal and fluid flow histories associated with tectonic evolution of a sedimentary basin. Previously such work utilised Rb–Sr dating or a combination of Rb–Sr and K–Ar (Ohr et al., 1991; Uysal et al., 2001; Uysal et al., 2004; Golding et al., 2006; Uysal et al., 2011). Dating by the Sm–Nd method was also integrated into these works, with varying success, due to its resistance to isotopic resetting compared to the Sr- or Ar-systems and allowed dating of multiple periods of hydrothermal fluid flow (Stille and Clauer, 1986; Ohr et al., 1991; Bros et al., 1992; Schaltegger et al., 1994; Toulkeridis et al., 1998).

By utilising granite- and sediment-hosted authigenic illite from the Warburton–Cooper basins, this study aims to reconstruct their thermal and fluid flow history to provide insight into the Phanerozoic tectonic evolution of one of the world's more enigmatic basin systems. Temporal constraints on fluid flow and, therefore tectonic activity, derive from a combination of ^{40}Ar–^{39}Ar, ^{87}Rb–^{87}Sr and ^{147}Sm–^{143}Nd dating. Three-fold integrated geochronology of this variety has not yet been attempted for authigenic illite in the literature but has the potential to record multiple fluid flow events that may further delineate previously unrecorded periods of active tectonism (Stille and Clauer, 1986; Bros et al., 1992; Awwiller, 1994; Schaltegger et al., 1994; Zwingmann et al., 1999; Uysal et al., 2001).

1.1 Geological Setting

The stacked Warburton–Cooper–Eromanga basins extend from south-east Queensland ca. 700 km into north-west South Australia (Fig. 1a) and comprise the early

Palaeozoic Warburton Basin, which is unconformably overlain by the Permian-Carboniferous Cooper and Jurassic-Cretaceous Eromanga basins. At the base of the Warburton Basin are the Cambrian, bimodal Mooracoochie Volcanics, including the 'Jena' basalt, unconformably overlain by mid-upper Cambrian shales and carbonates and Ordovician siltstones and shales (Gatehouse, 1986; Meixner et al., 1999). The Warburton Basin succession is intruded by the Big Lake Suite (BLS) granite that was previously thought to be associated with the Alice Springs Orogeny (Sun, 1997) and dated at 298 ± 4 and 323 ± 5 Ma (preferred SHRIMP ages) from the Moomba 1 and McLeod 1 wells, respectively (Gatehouse et al., 1995). The BLS has two predominant cupolas that comprise the "Moomba High" that is bounded by normal faults (Apak et al., 1995).These cupolas (Fig. 1b) are unusually enriched in heat-producing and/or radioactive elements: K, Th and U (up to 144 ppm Th and 30 ppm U; Middleton et al., 2013). The origin of enrichment is currently unknown, but has lead to substantial research and attempts to utilise the BLS for hot dry-rock geothermal energy (Chopra and Wyborn, 2003). The Warburton Basin is interpreted to have formed in a back-arc basin setting to the west of the Mt. Wright arc, inferring the presence of westward subduction (Roberts et al., 1990). Unconformably overlying the Warburton Basin and BLS granite are the Cooper and Eromanga basins that are arguably considered as intra-continental, sag basins (Apak et al., 1997; Cook et al., 2013).

The Gidgealpa–Merrimelia–Innamincka (GMI) Ridge is the most prominent NE–SW trending anticlinal thrust structure that is interpreted as Late Carboniferous, and divides the Patchawarra and Nappamerri synclinal troughs of the Cooper Basin (Sun, 1997; and references therein). The Cooper Basin developed structurally by the reactivation of previous faults until a period of tectonic quiescence. During this time, fluviatile, lacustrine and coal-bearing sequences were deposited until the mid Triassic (Apak et al., 1997; Mavromatidis, 2006). Sedimentation then ceased due to northeast-southwest apparent

compression, resulting in basin-wide exhumation and emplacement of the Nappamerri Unconformity (Thornton, 1979; Kuang, 1985). Subsequent subsidence and sedimentation of the Eromanga Basin deposited near uniform Jurassic to Cretaceous fluvial-lacustrine and shallow marine sediments until exhumation at the Upper Cretaceous–Palaeogene boundary. The following 90 Ma are characterised by minimal sedimentation and multiple periods of exhumation (Mavromatidis, 2006; Mavromatidis, 2008).

1.2. Sampling and analytical procedures

Authigenic illite–smectite samples were collected from multiple drill holes of structurally representative sites along the GMI Ridge and within the Nappamerri Trough (Fig. 1). Twelve samples were taken from Warburton Basin sediments along the GMI Ridge (Gidgealpa 1, Merrimelia 1 – 3, Tirrawarra 1, 7 and 10 and Wantana 1). A further 20 samples were taken from Warburton and Cooper sediments and the Big Lake Suite granite of the Nappamerri Trough (Moomba 1, 2, 7 and 72, Big Lake 1 and 57 and McLeod 1). As samples are taken from Warburton and Cooper Basin stratigraphy, they will be collectively referred to as Nappamerri Trough or GMI Ridge samples throughout the paper. If referring to an entire drill hole of samples, only the drill hole name (with no specific depth) will be given, for example MB_72 for Moomba 72 or BL_1 for Big Lake 1.

Thin section studies on whole-rock samples utilised a combination of plane–cross-polarised light, scanning electron microscopy with energy dispersive X-ray spectroscopy (SEM–EDS) and transmission electron microscopy (TEM). SEM–EDS analysis used the JEOL JXA-8500F (Hyperprobe) at the Deutsches GeoForschungsZentrum (GFZ) in Potsdam, Germany. TEM examination was made with the JEOL 2100 TEM at The

University of Queensland on nearly pure illite separates from the GMI Ridge (sediments) and Nappamerri Trough (granite). Clay suspensions were diluted in distilled water, disaggregated in an ultrasonic bath, and allowed to dry on carbon-coated copper grids. Further petrographic analyses were carried out using XRD on whole-rock and clay separates samples (<2 μm). The XRD analyses were carried out on a Bruker Advance MK III X-Ray diffractometer with Bragg-Brentano geometry and CuKα radiation, operated at 40 kV and 30 mA at a scanning rate of 1min/step and 0.05°/step from 2–32° for oriented clay slides. Polytype analyses were, however, operated at 40 kV and 30 mA at a scanning rate of 30secs/step and 0.05°/step from 16–44°. Samples were prepared for clay-fraction separation by gently hand-crushing the rocks to sand size to avoid artificially reducing grainsize of detrital/primary mineral components. Samples were then disaggregated in distilled water using an ultrasonic bath. Different clay size fractions (2–1, <1, 2–0.5 and <0.5 μm) were obtained by centrifugation, and the decanted suspensions were placed on a glass slide. To ensure no detrital contamination, samples were centrifugally separated and rigorously analysed with XRD. While $2M_1$ illite can form under high-temperature hydrothermal conditions (Zwingmann et al., 2010), it is indistinguishable from $2M_1$ primary muscovite. As such, samples showing $2M_1$ illite–muscovite components were either discarded from analysis or separated to finer micrometer fractions to avoid potential detrital/primary contamination. Following XRD analysis of air-dried samples, the oriented clay-aggregate mounts were placed in an ethylene–glycol atmosphere at 30–40 °C overnight prior to additional XRD analyses. To determine illite content in illite–smectite mixed-layer clays, the method of differential two-theta (Δ2θ) was used, with an analytical error of about ±5% (Moore and Reynolds, 1997).

Clay samples were dissolved with a mixture of HF and nitric acids on a hotplate, then evaporated to dryness, refluxed twice with nitric acid and dissolved in 2 *N* nitric acid. Aliquots of the solutions were spiked with internal standards (12 ppb Li, 6 ppb

Ni, Rh, In and Re, Bi and U), diluted and analysed on a Thermo X-series 1 quadrupole inductively coupled plasma mass spectrometer (ICP-MS) in the Radiogenic Isotope Laboratory at the University of Queensland (RIF, UQ). Sample preparation and analytical procedures used were similar to those of Eggins et al. (1997), except that Tm was not used as an internal standard and duplicate low-pressure digestions of W-2, a US Geological Survey diabase standard, were used as the calibration standard. BIR-1, AGV1, AGV2 and G2 were run as unknowns. The $^{156}CeO/^{140}Ce$ ratio for the run was 0.016. Long-term precision (RSD) was based on duplicate analyses of the duplicate digestions of AGV1, whilst precision for the run was based on five duplicate analyses of W-2 that were better than 3% for most elements, except for Li, Zn, Mo, Cd, and Cs, which ranged between 5% (Li, Cd and Cs) and 15% (Zn).

For the Rb–Sr dating, illitic clay separates were leached for 15 min at room temperature in 1 N distilled HCl (Clauer et al., 1993). Leachate and residue were separated using a centrifuge. The residue was rinsed repeatedly with milli-Q water, dried and reweighed with a five decimal point Sartorius MC1 balance. Clay separates were analysed in two separate batches. Leachate, residue, and untreated samples from the first batch were spiked with ^{85}Rb–^{84}Sr mixed tracer and dissolved in a mixture of distilled HF and HNO_3, whilst the second batch were measured directly by Thermo X-series 1 quadrupole ICP–MS with precision better than 0.5% (1σ). The Sr-enriched fraction was separated using cation exchange resins. Sr isotopic ratios were measured on a VG Sector-54 thermal ionisation mass spectrometer (TIMS) at RIF, UQ. Sr was loaded in TaF_5 and 0.1 *N* H_3PO_4 on a tantalum or tungsten single filament. Sr isotopic ratios were corrected for mass discrimination using $^{86}Sr/^{88}Sr = 0.1194$. Long-term (6 years) reproducibility of statically measured NBS SRM 987 (2σ; $n = 442$) is 0.710249 ± 28. More recent dynamically measured SRM 987 had $^{86}Sr/^{88}Sr$ ratios of 0.710222 ± 20 (2σ; $n = 140$). Rb–Sr isochron ages were calculated using the ISOPLOT program (Ludwig, 2003).

Samples chosen for Nd isotope analysis used aforementioned untreated, leachate and acid-leached fractions. These aliquots were separated for Nd following standard cation exchange column chemistry. Neodymium was separated from the REE fraction using Bio Bead® - HDEHP resin and eluting with 0.25 *N* HCl. Nd isotopes were determined using the multi-collector inductively coupled plasma mass spectrometer (MC-ICP-MS) in dynamic mode on a Nu Plasma MC-ICP-MS at RIF, UQ. Nd isotope ratios were corrected for mass fractionation using $^{146}Nd/^{144}Nd = 0.7219$. Repeated measurements of JNdi Nd standard on this mass spectrometer yield an average $^{143}Nd/^{144}Nd = 0.512113 \pm 9$ (2σ; $n = 11$), which is consistent with a consensus value of 0.512115 ± 7 (Tanaka et al., 2000). An in-house lab standard, Ames Nd Metal was used as a routine instrument drift monitor, correspondent with JNDi-1, 17 analyses yield an average of $^{143}Nd/^{144}Nd = 0.511966 \pm 16$. This value was used as calibration reference for instrument drift, which is usually less than 15ppm. The Nd procedural blank is ~50 pg.

A total of 7 samples from the Nappamerri Trough ($n = 5$) and GMI Ridge ($n = 2$) were dated by the ^{40}Ar–^{39}Ar method at the University of Michigan. Illitic clay samples were resuspended in 1 mL of deionized water, spun-down at 10,000 rpm in a microcentrifuge and carved into a ~1mm pellet following decanting. To avoid loss of ^{39}Ar due to recoil, clay pellets were placed in 1mm ID fused silica vials prior to being sent for neutron irradiation for 90MWh in medium flux locations of the McMaster Nuclear Reactor (hole 8C for irradiation 1, 8A for irradiation 2). Following irradiation, samples were attached to a laser fusion system, broken under a 1 x 10^{-8} Torr vacuum and step-heated *in situ* using a defocused beam from a 5 W Coherent Innova continuous Ar-ion laser operated in multi-line mode. Argon isotopes were then analysed using a VG1200S mass spectrometer equipped with a Daly detector operated in analogue mode using methods by Hall (2013). Ages in this study are calculated

relative to an age of 520.4 Ma for standard hornblende MMhb-1(Samson and Alexander, 1987).

2. RESULTS

2.1. Petrography and clay mineralogy

The Big Lake Suite granite shows intense illite-rich alteration resulting in almost complete destruction of primary feldspars and micas with pervasive illitic veinlet networks. Sediment samples, however, show less intense alteration with the majority of sediment-illite occurring as alteration products of detrital feldspar and mica or minor grain-coating. More detailed petrographic descriptions can be found in Middleton et al. (in prep.).

X-ray diffraction analysis identified two different types of illite–smectite throughout the Nappamerri Trough and GMI Ridge. All granite and most sediment-hosted illites show 001 peaks of ~10Å with minimal to no shift of the position upon ethylene glycolation. This indicates >95% illite typical of $R \geq 3$ Reichweite-type with long-range ordering. The remaining sediment-hosted illite–smectite (Mer1_3144 and BL57_1748) show shifts in the 001 peak from 9.7 – 9.6 Å after glycolation, with broad shoulders from 11 – 12 Å. Such XRD patterns reflect illite–smectite with 80 – 90% illite on the border of short-range and long-range ordering (R = 1 – $R \geq 3$; Reynolds and Hower, 1970; Moore and Reynolds, 1997).

Selected granite-hosted samples were chosen for polytype analysis to guarantee no contamination from inherited $2M_1$ muscovite. Primary $2M_1$ muscovite can be

isotopically reset during interaction with hydrothermal fluids, and thus record authigenesis (Zwingmann et al., 2010). However, if $2M_1$ muscovite is partially reset or unaffected during fluid flow then their incorporation into the study will produce inaccurate age data for authigenesis. All random powder XRD polytype analyses from Nappamerri Trough samples show diagnostic peaks (4.35, 4.12, 3.66, 3.07 and 2.93 Å) of authigenic trans-vacant 1M illite (Fig. 2a; Moore and Reynolds, 1997). Peaks show well-defined narrow reflections with no abnormal background levels between 20 and 35° 2θ, ruling out the presence of disordered $1M_d$ polytype. Transmitted electron microscopy was undertaken for those granite-hosted samples as well as selected sediment-hosted samples from the GMI Ridge. Photomicrographs of granite-hosted illite samples show stacked well-defined idiomorphic lath-like crystallites. Individual crystallites from MB72_3011.1 and MB72_3012 show no observable irregular edges and are interpreted to be authigenic (Fig. 2b; Hunziker et al., 1986; Reuter and Dallmeyer, 1987). Crystallites from MB1_2847.75 (granite; Fig. 2c) and Mer1_2653 (GMI Ridge sediment; Fig. 3), however, show a combination of idiomorphic and rounded grains indicating partial dissolution during multiple fluid flow events.

2.2. Geochronology of illitic clays from the Nappamerri Trough

2.2.1. Sm–Nd dating

Samarium and neodymium isotopic analyses were carried out on selected untreated and acid-leached aliquots from MB_72 granite-hosted illite samples. Samples were chosen on the basis of highly variable rare earth element compositions to give a wide enough range of Sm/Nd ratios appropriate for this dating method (Peng et al., 2003). A summary of

element and isotopic data is given in Figure 4 and Table 1. When plotted together, samples produce a meaningful $^{147}Sm/^{144}Nd$–$^{143}Nd/^{144}Nd$ isochron. Samples show a non-linear relationship on a 1/Nd vs. $^{143}Nd/^{144}Nd$ diagram, therefore eliminating the possibility the age data represent a two-fluid mixing-line. The isochron age is 128 ± 16 Ma (2σ) with an intercept of 0.512212 ± 17 (initial εNd = –8.3). Using measured $^{143}Nd/^{144}Nd$ values and the acquired Cretaceous age, Nd isotopic compositions were calculated for the time of formation. The initial isotopic values are presented in Table 1 in the epsilon (ε) notation using calculations after McCulloch and Wasserburg (1978) with $^{147}Sm/^{143}Nd$ CHUR (Chondritic Uniform Reservoir), present = 0.1967 (Jacobson and Wasserburg, 1980) and $^{143}Nd/^{144}Nd$ CHUR = 0.512638 (Goldstein et al., 1984). $\varepsilon Nd_{(128)}$ values vary minimally and range from –5.6 to –4.9.

2.2.2. Rb–Sr dating

Rb–Sr data for untreated, leachate and acid-leached (residue) clay separates, of varying size fraction (μm) were obtained for granite and sediment samples from the Nappamerri Trough (Table 2). Plotting all data on a single $^{87}Rb/^{86}Sr$–$^{87}Sr/^{86}Sr$ diagram shows a linear relationship for residues and evidence of partial isotopic disturbance of leachates from samples MB1, 2, 7 and McL1 that plot off isochrons (Fig. 5). Data from granite and sediment-hosted acid-leached residue clay fractions produced two linear relationships corresponding to potentially significant ages of 88.5 ± 2.8 Ma (initial $^{87}Sr/^{86}Sr$ =0.756 ± 0.014; MSWD = 1.8) and 101.1 ± 6.4 Ma (initial Sr^{87}/Sr^{86} = 0.775 ± 0.030; MSWD = 39) (Fig. 6a & b). However, if sediment-hosted samples from MB7 and McL1 are included in the younger isochron, both errors and MSWDs are substantially improved. This change provides ages of 86.6 ± 2.3 Ma (initial 0.7678 ± 0.0095; MSWD = 2.0) and 94.7 ± 4.2 Ma (initial

$^{87}Sr/^{86}Sr = 0.824 \pm 0.022$; MSWD = 0.40) with the latter made of samples wholly from MB72 (Fig. 6c & d). Selected leachate and untreated aliquots from MB_72 and BL_1 with anomalously high Sr^{87}/Sr^{86} values (0.9161 – 1.0357) produce a well-defined linear relationship with a mid Cretaceous age of 94.2 ± 1.8 Ma (initial Sr^{87}/Sr^{86} = 0.91357 ± 0.00091; MSWD = 1.9) and are parallel to the MB72 isochron (Fig. 6e).

4.2.3. Ar–Ar dating

Five granite-hosted illite samples of similar illite crystallinities were analysed for ^{40}Ar–^{39}Ar geochronology. Samples show 9.5–10.8% of low temperature ^{39}Ar "recoil loss" typical for well crystalline illite grains (Hall et al., 1997). Age data (1σ) is provided as total-gas or retention ages (Dong et al., 1995). The total-gas age refers to that produced from all the gas release from encapsulated samples, whilst the so-called retention age is the apparent ^{40}Ar–^{39}Ar age derived from all gases, excluding the first room-temperature gas fraction (recoil) in a vacuum-encapsulation experiment (Dong et al., 1995; Hall, 2013). Separates of 2–0.5μm fraction from MB1_2847.75 and MB1_2857.4 provide the youngest total-gas and retention ages of 93.3 ± 0.4 Ma and 102.8 ± 0.4 Ma (Fig. 7a), and 82.9 ± 0.6 Ma and 96.4 ± 0.7 Ma (Fig. 7b), respectively.Total degassing ages of MB_72 clays range from 96.6 ± 0.5 Ma to 102.3 ± 1.1 Ma with the oldest age belonging to the coarsest clay fraction of 1–2μm (Fig. 8a – c). Respective retention ages range from 107.9 ± 0.6 Ma to 112.8 ± 1.1 Ma. All samples have well developed plateaux that fall close-to (~45%) or within (>50%) the theoretical definition of Fleck et al. (50% of heating spectrum; 1977), and can be attributed to ^{39}Ar release from a single, homogenous reservoir (Clauer et al., 2012). However, the height of such plateaux do not necessarily represent geologically significant ages as age spectra can be significantly distorted by recoil artefacts such as the presence of point defects that are

created by recoiling ^{39}Ar nuclei (Hall et al., 2000). The same mechanism that caused enhanced degassing of ^{39}Ar in early gas fractions of a step-heating experiment, which in turn yield very low apparent ages, leads to a depletion of ^{39}Ar in the middle portion of the age spectrum. The resulting elevated ^{40}Ar/^{39}Ar ratios in the middle of the gas release biases apparent ages in what might be considered a plateau to values above the true age of the mineral. All Cl/K spectra for Nappamerri Trough samples indicate a large percentage of ^{38}Ar, derived from interaction with Cl (^{38}ArCl), is found in the low-temperature recoil fraction. A summary of all argon dating results are shown Table 3. Complete spectra with Ca/K, Cl/K and age plots are found, with respective ^{37}Ar, ^{38}Ar and data, in Appendices A and B, respectively.

2.3. Geochronology of illitic clays from the GMI Ridge

4.3.1. Rb–Sr dating

Rb–Sr data from the GMI Ridge were collected for illite from 9 sediment-hosted samples and are presented in Table 4. A combination of 7 untreated, 2 residue and 3 leachate illite separates produce an isochron with a corresponding age of 314.8 ± 9.4 Ma and initial ^{87}Sr/^{86}Sr of 0.7240 ± 0.0011 (MSWD = 18; Fig. 9a). Five acid-leached residue separates also provide a linear relationship with an age of 323.4 ± 9.4 Ma and an initial ^{87}Sr/^{86}Sr of 0.7200 ± 0.0012 (MSWD = 1.7; Fig. 9b). If aforementioned leachates are combined with different untreated (n = *2*) and residue (n = *1*) separates they produce a younger Late Triassic age of 201.7 ± 9.3 Ma (initial ^{87}Sr/^{86}Sr =0.7256 ± 0.0011; MSWD = 4.2; Fig. 9c).

4.3.2. Ar–Ar dating

The total-gas ^{40}Ar–^{39}Ar age for MER1_3144 (< 0.5 μm) from the GMI Ridge is 304.5 ± 1.1 Ma with a retention age of 366.6 ± 1.4 Ma (Fig. 10a and Table 3). A large discrepancy in ages derives from significant degree of recoil (18.5%). The age spectrum has a stepped appearance, with a plateau-like section at 0.31–0.53 ^{39}Ar fractions. Mer1_3039.5 (< 0.5 μm) produced younger Late Triassic ages of 191.4 ± 0.8 Ma (total-gas) and 231.8 ± 1.0 Ma (retention; Fig. 10b). The spectrum similarly shows stepped appearance with a plateau-like structure from 0.32–0.63 ^{39}Ar fractions. Age spectra climb to maxima between ~420 and ~450 Ma at total ^{39}Ar release. Both Cl/K spectra have stepped appearances with a large percentage of $^{38}ArCl$ release in the recoil fraction.

3. DISCUSSION

3.1. Interpretations of geochronology from the Nappamerri Trough

3.1.1. Sm–Nd dating

As the most resistant to isotopic resetting, the Sm–Nd records the oldest fluid flow event at 128 ± 16 Ma (Fig. 4; Schaltegger et al., 1994; Uysal et al., 2007). $\varepsilon Nd_{(128)}$ values of –5.6 to –4.9 indicate illite precipitation resulted from an influx of partially evolved basinal fluids and are similar to values previously reported for Cretaceous carbonate veins in the Nappamerri Trough (εNd(104) ~8.4; Middleton et al., under review). Studies on

authigenic carbonates and silicates have proven useful and consistently provide older Sm–Nd ages compared to Rb–Sr and Ar–Ar dating "Isotopic resistance" may stem from varying valencies, ionic radii and sites in the phyllosilicates structure of the Rb–Sr pair compared to Sm–Nd (Bros et al., 1992). As such, the isotopic systems could react differently during consequent fluid flow and partial recrystallisation under variable fluid/rock ratio. This phenomenon could, therefore, allow isotopically heterogeneous samples to simultaneously record more than one period of fluid flow.

31.2. Rb–Sr dating

Rb–Sr geochronology of granite- and sediment-hosted illites suggests the Nappamerri Trough underwent at least two fluid flow events in the Late Cretaceous recorded as two separate influxes of hydrothermal fluid. The first Cenomanian event is recorded by two parallel isochrons from MB72 samples, providing ages of 94.7 ± 4.2 Ma and 94.2 ± 1.8 Ma for residues and leachate–untreated separates, respectively (Fig. 6d & e). The abnormally elevated $^{87}Sr/^{86}Sr$ ratios exhibited by the leachate–untreated isochron, may derive from Cenomanian co-precipitation of K-rich leachable phases. An older age of 101.1 ± 6.4 Ma with high MSWD (MSWD = 39) reflects an incorrect inclusion of MB7 and McL1 sediment-hosted illites, which belong to a younger Coniacian hydrothermal event that reset the $^{87}Sr/^{86}Sr$ isotopic system (86.6 ± 2.3 Ma; Fig. 6c). The scatter of some leachable separates from both Cenomanian and Coniacian isochrons is compatible with isotopic disturbance from later fluid flow events (Fig. 5). Soluble leachable phases are commonly found in expandable and exchangeable interlayer sites as well as along basal surfaces of illites, thus are liable to disturbance from subsequent hydrothermal interaction (Ohr et al., 1991).

3.1.3. Ar–Ar dating

Interpreting ^{40}Ar–^{39}Ar spectra is not a simple task. This is partly due to the varying and conflicting schools-of-thought, which include interpreting stepped ^{39}Ar release spectra on the basis of multiple diffusion domains (Lovera et al., 1993; McDougall and Harrison, 1999; Cassata and Renne, 2013) or as mixed heterochemical domains (Villa, 2013; Villa and Hanchar, 2013). Likewise, the existence of plateaux/regular flat steps in heating spectra has many interpretations. While some earth scientists have attributed these features to discrete hydrothermal (Hall et al., 2000; Villa and Williams, 2013) or heating (van de Pluijm et al., 2001; Cassata and Renne, 2013; Piacentini et al., 2013) events, others have cast doubt on the geological meaningfulness of plateaux (Hodges et al., 1994; Sletten and Onstott, 1998; Forster and Lister, 2004). These intricacies are further exacerbated when analysing fine-grained mineral phases, such as illite, due to the degree of ^{39}Ar recoil that occurs during irradiation (Clauer et al., 2012). Recoil loss of ^{39}Ar is arguably dependent on factors such as the surface area of the analyzed aliquot, illite crystallinity (clay packet thickness), presence of structural defects and grain size (Hunziker et al., 1986; Reuter and Dallmeyer, 1987; Dong et al., 1995; Dong et al., 1997; Villa, 1997; Clauer et al., 2012; Clauer, 2013). To mitigate the complete loss of recoil ^{39}Ar, clay samples are encapsulated in quartz vials prior to irradiation. Moreover, typical interpretations of ^{39}Ar release spectra must be modified due a number of artefacts being introduced by ^{39}Ar recoil (see Hall et al. 2000). This includes an understanding that plateau height cannot be used as an age determinant as recoil commonly causes it to artificially overshoot geologically valid ages (Hall, 2013).

As samples are quartz vial encapsulated, ^{40}Ar–^{39}Ar illite age data can be in interpreted using total-gas ages or retention ages (Dong et al., 1995; Clauer et al., 2012). The retention age is calculated using ^{40}Ar and ^{39}Ar retained in the illite following irradiation, and

as such, omits the recoil gas fraction. This model assumes that any ^{39}Ar lost during encapsulated irradiation has come from the same sites from which ^{40}Ar was previously lost in nature (Dong et al, 1995; Hall et al., 2000). Total-gas ages are calculated using all the ^{39}Ar, including that lost due to recoil, and are equivalent to conventional K–Ar age measurements. Furthermore, total-gas ages assume that structural sites in illite crystallites, which are non-retentive of ^{40}Ar, are also devoid of K. Therefore, if any K resides in external, non-retentive sites of an illite packet, the recorded total-gas age will be an underestimate, providing a value below the correct age, and should be considered as a minimum age (Hall et al., 2000). Conversely, retention age calculations assume equal K concentrations are found in retentive and non-retentive sites of ^{40}Ar and hence, should be viewed as maximum ages (Dong et al., 1995; Hall et al., 1997; Hall et al., 2000; Clauer et al., 2012; Verdel et al., 2012)."

3.1.3.1 Retention age interpretation

Previous studies showed that retention ages proved more useful providing geologically significant ages for illitic clays with little smectite content that formed at higher temperatures (Dong et al., 1995; Dong et al., 1997). Inclusion of retention ages stretches illite formation from 112.8 ± 1.1 Ma to 96.4 ± 0.7 Ma (Fig. 7 & 8) suggesting a prolonged formational event of which the upper limit is within error of that recorded by Sm–Nd geochronology. On the other hand, excellent agreement between Rb–Sr isochron ages and ^{40}Ar–^{39}Ar total gas ages indicates both radiogenic ^{87}Sr and ^{40}Ar are retained within the illite structure to an exceptionally similar degree. This phenomenon is unsurprising as ^{40}Ar, K, Rb and Sr occupy the same interlayer space between 2:1 units (layers) of the clay structure (Dong et al., 1995). This implies that structural controls on ^{40}Ar retention in non-retentive sites during fluid-rock interaction and recrystallisation may similarly determine the retention

of radiogenic ^{87}Sr. For Rb–Sr isochron ages to be accurate, the analysed mineral must have the same retention for parent, ^{87}Rb, and radiogenic daughter, ^{87}Sr (Faure and Mensing, 2005). Simply put, crystallographic sites that are non-retentive of Rb should similarly contain zero ^{87}Sr. Thus, Rb–Sr ages should be considered minimum ages, just as with total gas. As such retention ages, which take into account the likely presence of K and Rb in non-retentive sites, may provide more accurate ages over those values given by total-gas or Rb–Sr method (Dong et al., 1995; Dong et al., 1997; Hall et al., 2000).

3.1.3.2. Total gas age interpretation

There is still substantial ambiguity surrounding the appropriate inclusion of retention ages when interpreting ^{40}Ar–^{39}Ar data. Dong et al. (2000) previously utilised a total gas model for diagenetic, smectite-rich illite–smectite. Conversely, they noted retention ages were in good agreement with depositional and Rb–Sr isochron ages for illite-rich clays from diagenetic, anchizonal and epizonal grades, distinguished by illite crystallinity values of >0.43, 0.43–0.26 and <0.26, respectively (Dong et al., 1995; Dong et al., 1997). Illite-rich (>95%) samples reported in this study fall within the diagenetic zone (IC values of ~0.56; Middleton et al., in prep.) but ^{40}Ar–^{39}Ar total-gas ages are remarkably consistent with Rb–Sr ages and, therefore, cast doubt on the retention age interpretation (Fig. 6c–e). In addition, by utilising a retention age model, invalidates the geological significance of acquired Rb–Sr ages (~94 Ma and ~86 Ma) that correspond perfectly with previously dated mixed-layered illite–smectite from the nearby Gunnedah (~94 Ma and ~86 Ma; Uysal et al., 2011), Galilee (~84 Ma) and Eromanga basins (~85 Ma; Uysal et al., in preparation).

Approximately 94 Ma Rb–Sr isochrons are within error of finer fractions (<1 μm) from MB_72, which give Ar–Ar total-gas ages of 96.6 ± 0.5 Ma to 96.7 ± 0.4 Ma. Total-

gas ages are from spectra with well-defined plateaux interpreted as ^{39}Ar release from homogenous reservoirs that recrystallised during a discrete fluid flow event (Fig. 8a & b). The high percentage of ^{38}ArCl released in the recoil gas fraction for all samples may result from interaction with a less than nanometre-sized, late-stage Cl-rich overgrowth (I.Villa pers. commun., 2014). Such a fine grain size is estimated on the basis of a mean recoil distance of ^{38}Ar of 1.1nm (140 eV; Onstott et al., 1995). Alternatively, coincident release of ^{38}ArCl with ^{39}ArK may suggest Cl is located in similar sites to recoiled ^{39}ArK, such as point defects and clay packet surfaces. Following the release of ^{39}Ar at low temperatures, all spectra also show a stepped overshoot above a plateau, which may derive from the enhanced mobility and excess loss of ^{39}Ar due to the high density of point defects during recoil (Hall, 2013). Such a hypothesis can also be invoked for the artificially older plateau age (Dong et al., 1997; Hall et al., 2000). The excessive loss of ^{39}Ar towards the end of the spectrum (i.e. high temperatures), may derive from a release of ^{39}Ar in highly retentive sites. Unlike the ~96 Ma spectra, the older 102 ± 1.1 Ma spectrum from a coarser MB_72 fraction (Fig. 8ce; 2–1 μm) has a two-tiered heating spectrum, with a high-step in the last 20% of ^{39}Ar release that could reflect gas release from multiple, heterochemical reservoirs (Zwingmann et al., 2001; Forster and Lister, 2004; Clauer et al., 2012; Villa, 2013). However, Ca/K ratios determined by the ^{37}Ar/^{39}Ar show little to no variation, implying ^{39}Ar release from phases of similar Ca and K content. On the other hand, Cl/K ratios show a distinctive increase coincident with the ^{39}Ar high-step, which likely reflects the decrepitation and degassing of Cl-rich fluid inclusions (Onstott et al., 1995; McDougall and Harrison, 1999).

Samples MB1_2857.4 (2–0.5 μm) and MB1_2847.75 (2–0.5 μm) fall on the 86.6 ± 2.3 Ma Rb–Sr isochron; however, they give relatively younger and older ^{40}Ar–^{39}Ar total-gas ages respectively.The younger age of 82.9 ± 0.6 Ma given by MB1_2857.4 (2–0.5 μm) could be due to prolonged hydrothermal circulation resulting in progressive closure of

Rb–Sr and K–Ar isotopic at decreasing temperatures (Fig. 7b). An alternative suggestion is that less crystalline illite in the 0.5 μm fractions contain a higher density of point defects allowing a lower retention and enhanced mobility of ^{40}Ar in nature giving erroneously young ages (Dong et al., 1995; Hall et al., 2000; Verdel et al., 2012). The relatively older ^{40}Ar–^{39}Ar total-gas age of 93.3 ± 0.4 Ma for sample MB1_2847.75 (2–0.5 μm) is not completely understood but may result from sample heterogeneity represented by more than one illite generation (Fig. 2c). A similar discrepancy in Rb–Sr and ^{40}Ar–^{39}Ar ages was seen for a collection of white micas from the Attic-Cycladic crystalline belt (Greece), where non-systematic distribution of Rb–Sr and ^{40}Ar–^{39}Ar ages resulted from heterogeneous metamorphic overprinting due to fluid–rock interactions under low fluid/rock ratios. (Bröcker et al., 2013). This could explain the disagreement in Rb–Sr and ^{40}Ar–^{39}Ar ages, as two separate sampling sessions of 2–0.5 μm separates incorporated into this study may have coincidently sampled both Cenomanian and Coniacian illites, respectively.

3.2. Interpretations of geochronology for the GMI Ridge

3.2.1. Rb–Sr dating

Rb–Sr dating of sediment-hosted illite from the GMI Ridge indicates two authigenic, fluid flow events in the Carboniferous and Jurassic. The oldest, Late Mississippian to Early Pennsylvanian age of 323.4 ± 9.4 Ma (Fig. 9b; MSWD = 1.7) is given by acid-leached residue and infers resistance to isotopic resetting following crystallisation. The younger 314.8 ± 9.4 Ma age with higher MSWD of 18 given by a combination of untreated, leachate and residue separates likely reflects a mixed age attributed to more than

one period of authigenesis recorded by insoluble residues and highly soluble leachates (Fig. 9a). As such, leachate separates are interpreted to form part of the 201.7 ± 9.3 Ma isochron in tandem with previously unused residue and untreated separates (Fig. 9c). The date of 314.8 ± 9.4 Ma is, therefore, a combination of Carboniferous (323.4 ± 9.4 Ma) and Late Triassic (201.7 ± 9.3 Ma) isochrons and has no geological significance.

3.2.2. Ar–Ar dating

Fine (<0.5 μm) clay fractions show a high degree of recoil with ~18% loss of ^{39}Ar during irradiation, consistent with the higher density of internal defects found in finer less crystalline clay separates (Fig. 10a & b; Hall, 2013). The stepped appearance of age and Cl/K spectra is commonly seen in samples that are composed of multiple, potentially detrital, heterochemical grains of varying age and grain-size, which were not identifiable with XRD (Haines and Van de Pluijm, 2010; Villa, 2013; Villa and Hanchar, 2013). Following recoil, low temperature steps result from extraction of ^{39}Ar from the least-retentive authigenic grains followed by progressive release from more retentive detrital grains at higher temperatures (Verdel et al., 2012). Under the assumptions of Verdel et al. (2012), the maximum age reached on the heating-spectrum may provide a minimum age estimate for those detrital phases.

The maximum ages of ~420–450 Ma seem reasonable as previous dating of vein carbonates and zircon from the Warburton Basin produce ages between 420 and 437 Ma associated with magmatic extensional activity during the Benambran Orogeny (Middleton et al., under review). Due to the stepped appearance of step-heating spectra and likely inclusion of detrital grains, the total-gas and retention ages of these encapsulated samples are not geologically meaningful. The similar total-gas age of 191.4 ± 0.8 Ma (Mer1-3039.5;

<0.5 μm) and Rb–Sr age of 201.7 ± 9.3 Ma may, therefore, result from natural ^{40}Ar loss subsequent to crystallisation, producing too young an age, in conjunction with detrital contamination that typically causes an overestimation of total-gas age. Assuming Rb–Sr ages are geological significant, the total-gas age of 304.5 ± 1.1 Ma for sample MER1_3144 (<0.5 μm) most likely results from a mixing of Jurassic and Carboniferous authigenic phases with a detrital Silurian component.

3.3. Geological Implications of illite ages

3.3.1. Nappamerri Trough

Integrated geochronology indicates that only the Nappamerri Trough underwent episodic fluid flow for ~35 Ma (~128–86 Ma; Fig. 11) during the Cretaceous, which was most likely localised along reactivated fault systems (Mavromatidis, 2008). This is also seen from widely distributed R ≥ 3 illite (>95%) with idiomorphic–rounded crystallites, that indicate partial dissolution of unstable illite grains during subsequent fluid–rock interaction. This period is coincident with previous thermochronological studies that record a substantial "recrystallisation event" of K-feldspar from the BLS, at ≤260°C from 120–80 Ma attributed to "rapid sediment accumulation and probably structural modification" (McLaren and Dunlap, 2006). As K-feldspar acts as an efficient "hygrochronometer" (Villa, 2013; Villa and Hanchar, 2013), previously noted recrystallisation likely relates to an episodic ingress of hydrothermal fluids capable of perturbing local geothermal gradients (Uysal et al., 2000). Thermal perturbations (≤ 350 °C) were also recognised from ~100–85 Ma and resulted in the maturation–expulsion of substantial quantities of hydrocarbons into the dry-gas zone

(Kantsler et al., 1978; Deighton and Hill, 1998). Maturation of kerogen to this extent can be produced from either a long-lasting diagenetic event or a high-temperature short-term thermal episode, consistent with multiple stages of Cretaceous tectonism (Derkowski et al., 2013). An elevated thermal regime associated with extension and an influx of hydrothermal fluids may, therefore, have provided sufficient heat to stimulate hydrocarbon maturation–expulsion (Allen and Allen, 2005; Middleton et al., 2013). Further evidence of extensional tectonism is seen from widespread normal faults throughout mid-Cretaceous Winton and Mackunda formations of the Eromanga Basins (Mavromatidis, 2008) as well as thickening of the volcanogenic, Winton Fm (Cook et al., 2013), which was dated at ~105–95 Ma from detrital zircon studies (Bryan et al., 2012).

The Cretaceous illite ages are consistent with extensive rifting of the southern and eastern margins of Australia, concomitant with emplacement of the Whitsunday silicic large igneous province (130–95 Ma; Bryan et al., 2012) (Fig. 12). Rifting along the eastern Australian margin (>2500 km) east of the study area was initiated suddenly at ~130–120 Ma along a N–S orientated volcanic rift system (Bryan et al., 1997), coincident with our Sm–Nd age of 128 ± 16 Ma. The ~94 Ma ages provided by ^{40}Ar–^{39}Ar and Rb–Sr data for 1–2 μm illites are also in agreement with accelerated rifting and exhumation beginning at ~100 Ma along the eastern Australian margin (O'Sullivan et al., 1995). The youngest generation of illite, dated between ~82 and ~86 Ma similarly coincides with rupture of the continental crust and onset of Tasman sea-floor spreading (~84 Ma; Veevers et al., 1991; Bryan et al., 2012), which was also recorded by Rb–Sr dating in the Gunnedah Basin of eastern Australia (~86 and 94 Ma; Uysal et al., 2011). Episodic fluid flow is also suggested by the depth-related distribution of radiometric ages in the BLS granite. As ~86 Ma illites are predominantly resticted to depths of ~2850 m, the 94 Ma fluid flow event may have sufficiently reduced

permeability restricting subsequent circulation of fluids to shallower, more permeable areas of the granite.

Chronological consistency with Gondwana rifting may suggest plate-wide transmission of tensional stress, commonly associated with break-up and dispersal, to previous thermally and mechanically weakened lithosphere (Coblentz and Sandiford, 1994; Friedmann and Burbank, 1995; Armitage and Allen, 2010). Thermal weakening of the Warburton–Cooper basins likely derives from high geothermal gradients associated with emplacement and high radiogenic heat-production (~12μWm^{-3}) of the BLS. On the other hand, mechanical weakening may stem from episodic compression–extension that lead to the formation of the GMI Ridge and accommodated emplacement of the BLS granite (Sonder et al., 1987; Braun and Beaumont, 1989). This hypothesis is also consistent with quantitative modelling of Müller et al. (2012) who showed that localised intraplate structural events of the Cretaceous derive from interaction of far field stresses with particularly weak zones of the Australian continent.

3.3.2. GMI Ridge

Age data indicates illite records of Carboniferous and Jurassic thermal events are restricted wholly to the GMI Ridge (Fig. 11). This may suggest that Cretaceous fluid flow in the Nappamerri Trough, was pervasive enough to overprint previously set isotopic values. The Rb–Sr age of 323.4 ± 9.4 Ma coincides with a published zircon SHRIMP age of 323 ± 5 Ma for the emplacement of the BLS (Fig. 13; Gatehouse et al., 1995). Illite dating and ^{40}Ar–^{39}Ar thermochronology of K-feldspar support an elevated thermal regime during the Pennsylvanian, which is attributed to incremental intrusion of the BLS (McLaren and Dunlap, 2006). This thermal regime may be related the last stages of the Alice Springs Orogeny

(ASO), which affected large portions of central Australia from 450–300 Ma (Haines et al., 2001). Alternatively, high geothermal gradients may result from emplacement of the BLS in an extensional setting. This would allow not only lateral accommodation of granitic melt (Petford et al., 2000), but also the influx and circulation of basinal fluids. This is consistent with normal faulting along the "Moomba High" (Apak et al., 1995) and Pennsylvanian extension throughout central to eastern Queensland. Such extension lead to widespread emplacement of silicic intrusions within the Kennedy–Connors–Auburn Province (Allen et al., 1998; Donchak et al., 2013) and development of the Galilee Basin Koburra Depocentre (Van Heeswijck, 2010). Such tectonism may, therefore, relate to the initial stages of the Early Permian Eastern Australian Rift System that affected up to 3000km of the eastern Australian coastline as a result of far-field backarc rifting that propagated from the west-dipping subduction zone of East Gondwanaland (Korsch et al., 2009).

A Late Triassic age (201.7 ± 9.3 Ma) suggests the Eromanga Basin experienced a significant diagenetic event (Zwingmann et al., 2001), capable of circulating basinal fluids along highly permeable, reactivated fault systems. Age data are coincident with the ~30 Ma Nappamerri Unconformity that marks cessation of the Cooper Basin and formation of the Eromanga Basin (Fig. 13; Mavromatidis, 2008). The formation of the Eromanga Basin is rather speculative and poorly-understood, with traditional hypotheses viewing it as an intracratonic 'sag' basin (Gallagher, 1990; Cook et al., 2013). Queensland experienced significant extension towards the end of the Late Triassic (Cook et al., 2013). This was responsible for the formation of a multitude of small, fault-bounded sedimentary basins across the former Bowen Basin that may have extended further west, influencing the thermal and fluid flow regime of the Eromanga Basin (Fielding, 1996; Uysal et al., 2001).

3.4. Significance of three-fold geochronological analysis

Previous studies have shown the Sm–Nd system to be useful in dating low-temperature sediment diagenesis due to its resistance to isotopic disturbance (Stille and Clauer, 1986; Ohr et al., 1991; Bros et al., 1992; Schaltegger et al., 1994). As seen from this study, the Sm–Nd method can also be extended to intermediate-temperature, hydrothermal systems experiencing variable fluid/rock ratios such as those noted in the Nappamerri Trough. Inclusion of the Sm–Nd isotopic system in geochronological studies, therefore, allows a better understanding of the temporal constraints on fluid flow and thus, regional tectonic activity from which it may derive. However, Sm–Nd dating of authigenic illite commonly provides less precise age data compared to the Rb–Sr and ^{40}Ar–^{39}Ar techniques (Awwiller, 1994; Schaltegger et al., 1994; Toulkeridis et al., 1998). This derives from relatively low concentrations of rare earth elements, a narrow range of Sm/Nd ratios and a particularly long half-life (106 Ga; Faure and Mensing, 2005).

As Sr- and Ar-isotopes can experience coincident hydrothermal resetting, utilising both methods provides complementary data during interpretation of geochronological analyses. In this study, Rb–Sr ages of Cretaceous illites are arguably more consistent with total-gas ages than retention ages. This phenomenon is contrary to Hall et al. (2000) who noted that retention ages were more useful than total-gas ages for illite–smectite with little to no smectite. Inconsistency of retention ages with Rb–Sr dating could result from minimal concentration of K^+ in non-retentive sites compared to retentive sites. As such, the amount of ^{40}Ar produced (by decay) in non-retentive sites is not equal to the amount of ^{39}Ar produced during neutron reaction. This could suggest that calculating the retention age, by omission of the recoiled gas fraction, should be done with caution for some illite formed in pervasive hydrothermal environments. The independent use of Rb–Sr and ^{40}Ar–^{39}Ar

geochronology to date hydrothermal illites is coupled with multiple geochemical assumptions. For example, to produce Rb–Sr isochrons with valid age data it is assumed that all analysed phases maintained uniform initial $^{87}Sr/^{86}Sr$ ratios. Unfortunately, the Rb–Sr method can suffer from certain geochemical pitfalls. This includes the production of geologically meaningless linear arrays/errorchrons from non-uniform initial $^{87}Sr/^{86}Sr$ ratios or from incorrectly plotting diachronous samples on the same isochron diagram, as seen in Figure 6a and b. However, separation of leachable and acid-leached residual phases during leaching experiments allows the identification and potential removal of isotopically disturbed leachates, thereby improving the accuracy of geologically meaingful isochrons (Ohr et al., 1991).

$^{40}Ar–^{39}Ar$ dating benefits from high precision and the presence of heating-spectra that can help determine the extent of heterochemical contamination, as seen in this study. Despite these benefits, $^{40}Ar–^{39}Ar$ dating of illites is also negatively affected by geochemical pitfalls such as excess ^{40}Ar and enhanced Ar mobility due to point defects and disagreement between consistent use of retention or total-gas ages (Dong et al., 1995; Hall et al., 2000; Haines and Van de Pluijm, 2010; Clauer et al., 2012; Verdel et al., 2012). As such, we suggest that future geochronological studies of hydrothermal illites utilise both Rb–Sr and $^{40}Ar–^{39}Ar$ methods. These methods concurrently will not only constrain the presence of isotopically disturbed leachates and detrital contamination but can discern accuracy of retention versus total gas ages relative to Rb–Sr dating. Dating fluid flow and clay mineral authigenesis is of particular interest to the mining and petroleum industries. Specifically, successful hydrocarbon exploration requires an understanding of the timing of maturation, migration and entrapment of hydrocarbons (Zwingmann et al., 1998). As high-temperature fluid flow can induce kerogen maturation as well as hydrocarbon migration–entrapment, dating hydrothermally-derived syngenetic illite can provide vital information to

model/constrain hydrocarbon reservoir formation (Zwingmann et al., 1998; Zwingmann et al., 1999; Uysal et al., 2004). Therefore, utilisation of three-fold geochronology in the petroleum industry could accurately and precisely date multiple episodes of fluid flow/hydrocarbon migration by using isotopically robust Sm–Nd dating in tandem with Rb–Sr and ^{40}Ar–^{39}Ar techniques.

4. CONCLUSIONS

Using a three-fold (^{40}Ar–^{39}Ar, ^{87}Rb–^{87}Sr and ^{147}Sm–^{143}Nd) geochronological method this paper provides the most comprehensive record of the tectonic evolution of the Warburton–Cooper basins to date. Authigenic illite ages provide evidence for three periods of fluid flow coincident with previously recorded tectonism. The location of samples further indicates that while Carboniferous (323.4 ± 9.4 Ma) and Late Triassic (201.7 ± 9.3 Ma) events were basin-wide, Cretaceous (~128 to ~86 Ma) fluid flow was episodic and restricted to the synclinal Nappamerri Trough. Furthermore, as the Warburton–Cooper basins are distant from active plate margins, recorded fluid flow associated with regional tectonism likely derives from localisation of far-field stresses to thermally and mechanically weakened regions of the Australian continent. Such weaknesses may stem from continual reactivation of fault networks as well as considerable heat-production (~12μWm^{-3}) from the highly radioactive BLS granite. By combining ^{40}Ar–^{39}Ar, ^{87}Rb–^{87}Sr and ^{147}Sm–^{143}Nd dating of illite, this study not only delineates episodic fluid flow but also reduces problems/weaknesses commonly faced when utilising radiometric dating techniques.

Acknowledgments

The authors acknowledge the Government of South Australia and Geodynamics Ltd. for granting permission to sample core. We thank Dr. Yeu-xing Feng, Dr. Irena Kinaev, Dr. Ai Duc Nguyen, Dr. Hans-Jürgen Förster and Dr. Dieter Rhede for their help with analytical work and technical assistance. Special thanks go to Turgay Demir for his assistance during sample preparation. Microscopy was undertaken at Deutsches GeoForschungsZentrum, Potsdam, as part of a collaborative research agreement between this Federal Research Institute and The University of Queensland, Australia. The authors acknowledge the facilities, and the scientific and technical assistance, of the Australian Microscopy & Microanalysis Research Facility at the Centre for Microscopy and Microanalysis, The University of Queensland. Prof. Paulo Vasconcelos, Dr. David Thiede and Dr. Charles Verdel are thanked for constructive comments during the initial stages of this paper. I. Villa, G. S. Lister and an anonymous reviewer are thanked for thoughtful and constructive reviews of the manuscript.

References

Allen, C. M., Williams, I. S., Stephens, C. J., and Fielding, C. R., 1998. Granite genesis and basin formation in an extensional setting: The magmatic history of the Northernmost New England Orogen. *Aust. J. Earth Sci.* **45**, 875–888.

Allen, P. A. and Allen, J. R., 2005. *Basin analysis: principles and applications*. Blackwell Science Ltd., Oxford.

Apak, S. N., Stuart, F., Lemon, N. M., and Wood, G., 1997. Structural evolution of the Permian–Triassic Cooper Basin, Australia: Relation to hydrocarbon trap styles. *AAPG Bulletin* **81**, 533–555.

Apak, S. N., Stuart, W. J., and Lemon, N. M., 1995. Compressional control on sedimentation and facies distribution SW Nappamerri Syncline and adjacent Murteree High, Cooper Basin. *The APEA Journal* **35**, 190-202.

APPEA, 2003. *Development and Production Statistics*. Australian Petroleum Production and Exploration Association Limited, Canberra.

Armitage, J. J. and Allen, P. A., 2010. Cratonic basins and the long-term sibsidence history of continental interiors. *J Geol Soc London* **167**, 61–70.

Awwiller, D. N., 1994. Geochronology and mass transfer in Gulf Coast mudrocks (south-central Texas, U.S.A.) : Rb–Sr, Sm–Nd and REE systematics. *Chem. Geol.* **116**, 61–84.

Braun, J. and Beaumont, C., 1989. Contrasting styles of lithospheric extension: Implications for differences between the Basin and Range province and rifted continental margins. In: Tankard, A. J. and Balkwill, H. R. Eds.), *Extensional Tectonics and Stratigraphy of the North Atlantic Margin*. AAPG.

Bröcker, M., Baldwin, S., and Arkudas, R., 2013. The geological significance of 40Ar/39Ar and Rb–Sr white mica ages from Syros and Sifnos, Greece: a record of continuous (re)crystallisation during exhumation? *J Metamorph Geol* **(in press)**.

Bros, R., Stille, P., Gauthier-Lafaye, F., Weber, F., and Clauer, N., 1992. Sm–Nd isotopic dating of Proterozoic clay material: An example from the Francevillian sedimentary series, Gabon. *Earth Planet. Sci. Lett.* **113**, 207–218.

Bryan, S. E., Constantine, A. E., Stephens, C. J., Ewart, A., Schön, R. W., and Parianos, J., 1997. Early Cretaceous volcano-sedimentary successions along the eastern Australian continental margin: Implications for the break-up of eastern Gondwana. *Earth Planet. Sci. Lett.* **153**, 85–102.

Bryan, S. E., Cook, A. C., Allen, C. M., Siegel, C., Purdy, D., Greentree, J. S., and Uysal, I. T., 2012. Early–mid Cretaceous tectonic evolution of eastern Gondwana: From silicic LIP magmatism to continental rupture. *Episodes* **35**, 142–152.

Cassata, W. S. and Renne, P. R., 2013. Systematic variations of argon diffusion in feldspars and implications for thermochronometry. *Geochim. Cosmochim. Acta* **112**, 251–287.

Chopra, P. and Wyborn, D., 2003. Australia's first hot dry rock geothermal energy extraction project is up and running in granite beneath the Cooper Basin, NE South Australia, *The Ishihara Symposium: Granites and Associated Metallogenesis*. 43-45. Macquarie, Australia.

Clauer, N., 2013. The K–Ar and $^{40}Ar/^{39}Ar$ methods revisited for dating fine-grained K-bearing clay minerals. *Chem. Geol.* **354**, 163–185.

Clauer, N., Chaudhuri, S., Kralik, M., and Bonnotcourtois, C., 1993. Effects of experimental leaching on Rb–Sr and K–Ar isotopic systems and REE contents of diagenetic illite. *Chem. Geol.* **103**.

Clauer, N., Zwingmann, H., Liewig, N., and Wendling, R., 2012. Comparative $^{40}Ar/^{39}Ar$ and K–Ar dating of illite-type clay minerals: A tentative explanation for age identities and differences. *Earth Science Reviews* **115**, 76–96.

Coblentz, D. D. and Sandiford, M., 1994. Tectonic stresses in the African plate: Constraints on the ambient lithospheric stress state. *Geology* **22**, 831–834.

Cook, A. G., Bryan, S. E., and Draper, J. J., 2013. Post-orogenic Meoszoic basins and magmatism. In: Jell, P. A. (Ed.), *Geology of Queensland*. Geological society of Queensland, Brisbane.

Deighton, I. and Hill, A. J., 1998. Thermal and burial history. In: Gravestock, D. I., Hibburt, J., and Drexel, J. F. Eds.), *Petroleum Geology of South Australia*. South Australia. Department of Primary Industries and Resources.

Derkowski, A., Bristow, T. F., Wampler, J. M., Środoń, J., Marynowski, L., Elliot, W. C., and Chamberlain, C. P., 2013. Hydrothermal alteration of the Ediacaran Doushantuo Formation in the Yangtze Gorges area (south China). *Geochim. Cosmochim. Acta* **107**, 279–298.

Donchak, P. J. T., Purdy, D. J., Withnall, I. W., Blake, P. R., and Jell, P. A., 2013. New England Orogen. In: Jell, P. A. (Ed.), *Geology of Queensland*. Geological Society of Queensland, Brisbane.

Dong, H., Hall, C. M., Halliday, A. N., Peacor, D., Merriman, R. J., and Roberts, B., 1997. $^{40}Ar/^{39}Ar$ illite dating of Late Caledonian (Acadian) metamorphism and cooling K-bentonites and slates from the Welsh Basin, UK. *Earth Planet. Sci. Lett.* **150**, 337–351.

Dong, H., Hall, C. M., Peacor, D., and Halliday, A. N., 1995. Mechanisms of argon retention in clats revealed by laser ^{40}Ar–^{39}Ar dating. *Science* **267**, 355–359.

Dong, H., Hall, C. M., Peacor, D., Halliday, A. N., and Pevear, D. R., 2000. Thermal 40Ar/39Ar separation of diagenetic from detrital illitic clays in Gulf Coast shales. *Earth Planet. Sci. Lett.* **175**, 309–325.

Eggins, S. M. W., J. D., Kinsley, L. P. J. M., G. E., Sylvester, P., McCulloch, M. T., Hergt, J. M., and Handler, M. R., 1997. A simple method for the precise determination of ≥ 40 trace elements in geological samples by ICPMS using enriched isotope internal standardisation. *Chem. Geol.* **134**, 311–326.

Faure, G. and Mensing, T. M., 2005. *Isotopes: Priniciples and applications*. John Wiley & Sons, Hoboken, New Jersey.

Fielding, C. R., 1996. Mesozoic sedimentary basins and resources in eastern australia – A review of current understanding, *Mesozoic Geology of the Eastern Asutralian Plate Conferene*. Geological Society of Australia, 43, 180–185. Brisbane.

Fleck, R. J., Sutter, J. F., and Elliot, D. H., 1977. Interpretation of discordant $^{40}Ar/^{39}Ar$ age-spectra of Mesozoic tholeiites from Antartica. *Geochim. Cosmochim. Acta* **41**, 15–32.

Forster, M. A. and Lister, G. S., 2004. The interpretation of $^{40}Ar/^{39}Ar$ apparent age spectra produced by mixing: application of the method of asymptotes and limits. *J. Struct. Geol.* **26**, 287–305.

Friedmann, S. J. and Burbank, D. W., 1995. Rift basins and supradetachment basins: intracontinental extensional end-members. *Basin Res.* **7**, 109–127.

Gallagher, K., 1990. Permian–Cretaceous subsidence history along the Eromanga–Brisbane geoscience transect. *Bulletin of the Bureau of Mineral Resources, Australia* **232**, 133–151.

Gatehouse, C. G., 1986. The geology of the Waburton Basin in South Australia. *Aust. J. Earth Sci.* **33**, 161–180.

Gatehouse, C. G., Fanning, C. M., and Flint, R. B., 1995. Geochronology of the Big Lake Suite, Warburton Basin, northeastern South Australia*Quarterly Geological Notes*. Geological Survey of South Australia, **128**, 8–16.

Gerdes, A. and Zeh, A., 2009. Zircon formation versus zircon alteration — New insights from combined U–Pb and Lu–Hf in-situ LA-ICP-MS analyses, and consequences for the interpretation of Archean zircon from the Central Zone of the Limpopo Belt. *Chem. Geol.* **261**, 230–243.

Golding, S. D., Uysal, I. T., Glikson, M., Baublys, K. A., and Southgate, P. N., 2006. Timing and chemistry of fluid-flow events in the Lawn Hill Platform, Northern Australia. *Econ. Geol.* **101**, 1231-1250.

Haines, P. W., Hand, M., and Sandiford, M., 2001. Palaeozoic synorogenic sedimentation in central and northern Australia: a review of distribution and timing with implications for the evolution of intracontinental orogens. *Aust. J. Earth Sci.* **48**, 911–928.

Haines, S. H. and Van de Pluijm, B. A., 2010. Dating the detachment fault system of the Ruby Mountains, Nevada: Singinficance for the kinematics of low-angle normal faults. *Tectonics* **29**, TC4028.

Hall, C. M., 2013. Direct measurement of recoil effects on $^{40}Ar/^{39}Ar$ standards. In: Jourdan, F., Mark, D. F., and Verati, C. Eds.), *Advances in $^{40}Ar/^{39}Ar$ dating: from Archaeology to Planetary Sciences*. Geological Society, London.

Hall, C. M., Higueras, P. L., Kesler, S. E., Lunar, R., Dong, H., and Halliday, A. N., 1997. Dating of alteration episodes related to mercury mineralisation in the Almadén district, Spain. *Earth Planet. Sci. Lett.* **148**, 287–298.

Hall, C. M., Kesler, S. E., Simon, G., and Fortuna, J., 2000. Overlapping Cretaceous and Eocene alteration, Twin Creeks Carlin-type deposit, Nevada. *Econ. Geol.* **95**, 1739–1752.

Hillis, R. R., Hand, M., Mildren, S., Morton, J., Reid, P., and Reynolds, S., 2004. Hot dry rock geothermal exploration in Australia, *PESA Eastern Australian Basins Symposium II*. Adelaide.

Hodges, K. V., Harries, W. E., and Bowring, S. A., 1994. $^{40}Ar/^{39}Ar$ age gradients in micas from a high-temperature-low-pressure metamorphic terrain: Evidence for very slow cooling and implications for the interpretation of age spectra. *Geology* **22**, 55–58.

Hunziker, J. C., Frey, M., Clauer, N., Dallmeyer, R., Friedrichsen, H., Flehmig, W., Hochstrasser, K., Roggwiler, P., and Schwander, H., 1986. The evolution of illite to muscovite: mineralogical and isotopic data from the Glarus Alps, Switzerland. *Contrib. Mineral. Petr.* **92**, 157–180.

Kantsler, A. J., Cook, A. C., and Smith, G. C., 1978. Rank variation, calculated palaeotemps understanding oil, gas occurrence. *Oil and Gas Journal* **Nov. 20**, 196–205.

Korsch, R. J., Totterdell, J. M., Cathro, D. L., and Nicoll, M. G., 2009. Early Permian Eastern Australian Rift System. *Aust. J. Earth Sci.* **58**, 381–400.

Kuang, K. S., 1985. History and style of Cooper–Eromanga Basin structures. *Exploration Geophysics* **16**, 245–248.

Lovera, O. M., Heizler, M. T., and Harrison, T. M., 1993. Argon diffusion domains in K-feldspar II: kinetic properties of MH-10. *Contrib. Mineral. Petr.* **113**, 381–393.

Ludwig, K. R., 2003. *Users manual for ISOPLOT/EX, version 3. A geochronological toolkit for Microsoft Excel.* Berkeley Geochronological Centre Special Publication.

Mavromatidis, A., 2006. Burial/exhumation histories for the Cooper-Eromanga Basins and implications for hydrocarbon exploration, Eastern Australia. *Basin Res.* **18**, 351–373.

Mavromatidis, A., 2008. Two layer model of lithospheric compression and uplift / exhumation in an intracratonic setting: an example from the Cooper–Eromanga Basins, Australia. *International Journal of Earth Science* **97**, 623–634.

McDougall, I. and Harrison, T. M., 1999. *Geochronology and thermochronology by the $^{40}Ar/^{39}Ar$ method*. Oxford University Press, New York.

McLaren, S. and Dunlap, W. J., 2006. Use of $^{40}Ar/^{39}Ar$ K-feldspar thermochronology in basin thermal history reconstruction: an example from the Big Lake Suite granites, Warbruton Basin, South Australia. *Basin Res.* **18**, 189–203.

Meixner, A. J., Boucher, R. K., Yeates, A. N., Gunn, P. J., Richardson, L. M., and Frears, R. A., 1999. Interpretation of geophysical and geological data sets, Cooper Basin region, South Australia. Australian Geological Survey Organisation.

Merriman, R. J. and Frey, M., 1999. Patterns of very low-grade metamorphism in metapelitic rocks. In: Frey, M. and Robinson, D. Eds.), *Low-grade metamorphism*. Blackwell Science, Cambridge.

Middleton, A. W., Uysal, I. T., Bryan, S. E., Hall, C. M., and Golding, S. D., 2013. Crustal evolution of the intracontinental Warburton–Cooper–Eromanga Basin system, central Australia. *Mineral. Mag.* **77**, 1754.

Middleton, A. W., Uysal, I. T., Golding, S. D., Förster, H.-J., and Rhede, D., under review. Integrated geochronology and geochemistry from the Waburton Basin, Australia: Deciphering a thermal history. *Chem. Geol.*

Moore, D. M. and Reynolds, R. C. J., 1997. *X-ray Diffraction and the Identification and Analysis of Clay Minerals*. Oxford University Press, Oxford.

Müller, R. D., Dyksterhuis, S., and Rey, P., 2012. Australian paleo-stress fields and tectonic reactivation over the past 100 Ma. *Aust. J. Earth Sci.* **59**, 13–28.

Nasdala, L., Hanchar, J. M., Rhede, D., Kennedy, A. K., and Váczi, T., 2010. Retention of uranium in complexly altered zircon: An example from Bancroft, Ontario. *Chem. Geol.* **269**.

O'Sullivan, P. B., Kohn, B. P., Foster, D. A., and Gleadow, A. J. W., 1995. Fission track data from the Bathurst Batholith: evidence for rapid mid-Cretaceous uplift and erosion within the eastern highlands of Australia. *Aust. J. Earth Sci.* **42**, 597–607.

Ohr, M., Halliday, A. N., and Peacor, D., 1991. Sr and Nd isotopic evidence for punctuated clay diagenesis, Texas Gulf coast. *Earth Planet. Sci. Lett.* **105**, 110–126.

Onstott, T. C., Miller, M. L., Ewing, R. C., Arnold, G. W., and Walsh, D. S., 1995. Recoil refinements: Implications for the $^{40}Ar/^{39}Ar$ dating technique. *Geochim. Cosmochim. Acta* **59**, 1821–1834.

Peng, J.-T., Hu, R.-Z., and Burnard, P. G., 2003. Samarium–neodymium isotope systematics of hydrothermal calcites from the Xikuangshan antimony deposit (Hunan, China): the potential of calcite as geochronometer. *Chem. Geol.* **200**, 129–136.

Petford, N., Cruden, A. R., McCaffrey, K. J. W., and Vigneresse, J.-L., 2000. Granite magma formation, transport and emplacement in the Earth's crust *Nature* **408**, 669–673.

Piacentini, T., Vasconcelos, P. M., and Farley, K. A., 2013. $^{40}Ar/^{39}Ar$ constraints on the age and thermal history of the Urucum Neoproterozoic banded iron-formation, Brazil. *Precambrian Research* **228**, 48–62.

Reuter, A. and Dallmeyer, R., 1987. Significance of Ar40/Ar39 age spectra of whole-rock and constituent grain-size fractions from anchizonal slates. *Chem. Geol.* **66**, 73–88.

Reynolds, R. C. J. and Hower, J., 1970. The nature of interlayering in mixed-layer illite-montmorillonites. *Clays Clay Miner.* **18**, 25–36.

Rezaee, M. R. and Sun, X., 2007. Fracture-filling cements in the Palaeozoic Warburton Basin, South Australia. *Journal of Petroleum Geology* **30**, 79–90.

Roberts, D. C., Carroll, P. G., and Sayers, J., 1990. The Kalladeina Formation - A Warburton Basin Cambrian carbonate play. *The APEA Journal* **30**, 166–184.

Samson, S. D. and Alexander, E. C. J., 1987. Calibration of the interlaboratory 40Ar/39Ar dating standard, MMhb-1. *Chemical Geology Isotope Geoscience* **66**.

Schaltegger, U., Stille, P., Rais, N., Piqué, A., and Clauer, N., 1994. Neodymium and strontium dating of diagenesis and low-grade metamorphism of argillaceous sediments. *Geochim. Cosmochim. Acta* **58**, 1471–1481.

Sletten, V. W. and Onstott, T. C., 1998. The effect of the instability of muscovite during in vacuo heating on $^{40}Ar/^{39}Ar$ step-heating spectra. *Geochim. Cosmochim. Acta* **62**, 123–141.

Sonder, L. J., England, P. C., Wernicke, B. R., and Christiansen, R. L., 1987. A physical model for Cenozoic extension of western North America. In: Coward, M. P., Dewey, J. F., and Hancock, P. L. Eds.), *Continental Extensional Tectonics*. Special Publication fo the Geological Society.

Stille, P. and Clauer, N., 1986. Sm–Nd isochron-age and provenance of the argillites of the Gunflint Iron Formation in Ontario, Canada. *Geochim. Cosmochim. Acta* **50**, 1141–1146.

Sun, X., 1997. Structural style of the Warburton Basin and control in the Cooper and Eromanga Basins, South Australia. *Exploration Geophysics* **28**, 333–339.

Tanaka, T., Togashi, S., Kamioka, H., Amakawa, H., Kagami, H., Hamamoto, T., Yuhara, M., Orihashi, Y., Yoneda, S., Shimizu, H., Kunimaru, T., Takahashi, K., Yanagi, T., Nakano, T., Fujimaki, H., Shinjo, R., Asahara, Y., Tanimizu, M., and Dragusanu, C., 2000. JNdi-1: a neodymium isotopic reference in consistency with LaJolla neodymium. *Chem. Geol.* **168**, 279–281.

Thornton, R. C. N., 1979. Regional stratigraphic analysis of the Gidgealpa Group, southern Cooper Basin, Asutralia. *Australian Geological survey Bulletin* **49**, 140–145.

Toulkeridis, T., Clauer, N., Chaudhuri, S., and Goldstein, S. L., 1998. Multimethod (K–Ar, Rb–Sr, Sm–Nd) dating of bentonite minerals from the eastern United states. *Basin Res.* **10**, 261–270.

Uysal, I. T., Glikson, M., Golding, S. D., and Audsley, F., 2000. The thermal history of the Bowen Basin, Queensland, Australia: vitrinite reflectance and clay mineralogy of Late Permian coal measures. *Tectonophysics* **323**, 105–129.

Uysal, I. T., Glikson, M., Golding, S. D., and Southgate, P. N., 2004. Hydrothermal control on organic matter alteration and illite precipitation, Mt Isa Basin, Australia. *Geofluids* **4**.

Uysal, I. T., Golding, S. D., Bolhar, R., Zhao, J.-X., Feng, Y.-X., Baublys, K., and Greig, A., 2011. CO_2 degassing and trapping during hydrothermal cycles related to Gondwana rifting in eastern Australia. *Geochim. Cosmochim. Acta* **75**, 5444–5466.

Uysal, I. T., Golding, S. D., and Thiede, D. S., 2001. K–Ar and Rb–Sr dating of authigenic illite–smectite in Late Permian coal measures, Queensland, Australia: implication for thermal history. *Chem. Geol.* **171**, 195–211.

Uysal, I. T., Mutlu, H., Altunel, E., Karabacak, V., and Golding, S. D., 2006. Clay mineralogical and isotopic (K-Ar, $\delta^{18}O$, δD) constraints on the evolution of the North Anatolian Fault Zone, Turkey. *Earth Planet. Sci. Lett.* **243**, 181-194.

Uysal, I. T., Zhao, J.-X., Golding, S. D., Lawrence, M. G., Glikson, M., and Collerson, K. D., 2007. Sm–Nd dating and rare-earth element tracing of calcite: Implications for fluid-flow events in the Bowen Basin, Australia. *Chem. Geol.* **238**, 63–71.

van de Pluijm, B. A., Hall, C. M., Vrolijk, P. J., Pevear, D. R., and Covey, M. C., 2001. The dating of shallow faults in the Earth's crust. *Nature* **412**, 172–174.

Van Heeswijck, A., 2010. Late Paleozoic to Early Mesozoic deformation in the northeastern Galilee Basin, Australia. *Aust. J. Earth Sci.* **57**, 431–451.

Veevers, J. J., Powell, C. M., and Roots, S. R., 1991. Review of seafloor spreading around Austrlia. 1. Synthesis of spreading. *Aust. J. Earth Sci.* **38**, 373–389.

Verdel, C., van de Pluijm, B. A., and Niemi, N., 2012. Variation of illite/muscovite $^{40}Ar/^{39}Ar$ spectra during progressive low-grade metamorphism: an example from the US Cordillera. *Contrib. Mineral. Petr.* **164**, 521–536.

Villa, I. M., 1997. Direct determination of ^{39}Ar recoil distance. *Geochim. Cosmochim. Acta* **61**, 689–691.

Villa, I. M., 2013. *Diffusion of Ar in K-feldspar: present and absent*. Geological Society of London.

Villa, I. M. and Hanchar, J. M., 2013. K-feldspar hygrochronology. *Geochim. Cosmochim. Acta* **101**, 24–33.

Villa, I. M. and Williams, M. L., 2013. Geochronology of metasomatic events. In: Harlov, D. E. and Austrheim, H. Eds.), *Metasomatism and the chemical transformation of rock: The role of fluids in terrestrial and extraterrestrial processes*. Springer Heidelberg, New York.

Zwingmann, H., Clauer, N., and Gaupp, R., 1998. Timing of fluid flow in a sandstone reservoir of the north German Rotliegend (Permian) by K–Ar dating of related hydrothermal illite. In: Parnell, J. (Ed.),*Dating and duration of fluid flow and fluid–rock interaction*. Special Publication, **144**, 91–106. Geological Society, London.

Zwingmann, H., Clauer, N., and Gaupp, R., 1999. Structure-related geochemical (REE) and isotopic (K–Ar, Rb–Sr, δ18O) characteristics of clay minerals from Rotliegend sandstone reservoirs (Permian, northern Germany). *Geochim. Cosmochim. Acta* **63**, 2805–2823.

Zwingmann, H., Mancktelow, N., Antognini, M., and Lucchini, R., 2010. Dating of shallow faults: New constraints from the AlpTransit tunnel site (Switzerland). *Geology* **38**, 487–490.

Zwingmann, H., Tingate, P., Lemon, N. M., and Hamilton, P. J., 2001. K–Ar dating, petrographic and thermal modelling constraints on illite origin in the Cooper Basin, South Australia. In: Hill, K. C. and Bernecker, T. Eds.), *Eastern Australasian Basins Symposium*. Petroleum Exploration Society of Australia, Special Publication, 321–327. Melbourne.

Figure Captions

Figure 1

Figure 1. (A) Location of the Warburton–Cooper–Eromanga Basin system in Australia. (B) Close-up view of sample area including locations of the Big Lake Suite granite plutons, drill-holes and the Gidgealpa (GR), Merrimelia (MR), Yanpurra (YR) and Innamincka (IR) ridge system.

Figure 2

Figure 2. Representative XRD pattern for 1M polytypes (A); and TEM photomicrographs of idiomorphic (B; MB72_3012) and rounded-edge and idiomorphic (C; MB1_2847.75) crystallites. The rounded-edge crystallites indicate partial dissolution of illite from preceding hydrothermal events, whilst idiomorphic crystallites indicate crystallisation from coincident fluid flow.

Figure 3

Figure 3. A TEM photomicrograph of idiomorphic rounded-edge and idiomorphic crystallites from sample Mer2_2653.4.

Figure 4

Figure 4. Sm–Nd isochron for selected residue and untreated clay separates from the Big Lake suite granite.

Figure 5

Figure 5. Combined $^{87}Rb/^{86}Sr$–$^{87}Sr/^{86}Sr$ diagram showing linear relationships for leachate–residue–untreated clay fractions for illite samples from Nappamerri Trough.

Figure 6

Figure 6. Rb–Sr isochrons of selected leachate–residue–untreated clay fractions for illite samples from Nappamerri Trough (granite and sediment; A–E).

Figure 7

Figure 7. ^{40}Ar–^{39}Ar step-heating for vacuum-encapsulated, granite-hosted illite of 2–0.5 μm (A & B; MB1_2847.75 & MB1_2857.4), where f_{recoil} refers to the fraction of ^{39}Ar lost during recoil. Age data are reported as retention and total-gas ages. Retention ages are calculated using ^{40}Ar and ^{39}Ar retained in the illite following irradiation, and as such, omits the recoil gas fraction (Dong et al, 1995; Hall et al., 2000). Total-gas ages are calculated using all the ^{39}Ar, including that lost due to recoil, and are equivalent to conventional K–Ar age measurements.

Figure 8

Figure 8. ^{40}Ar–^{39}Ar step-heating for vacuum-encapsulated, granite-hosted illite of < 1 μm (A & B; MB72_3009.9 & MB72_3012) and 2–1 μm (C; MB72_3011.1) clay fractions, where f_{recoil} refers to the fraction of ^{39}Ar lost during recoil.

Figure 9

Figure 9. Rb–Sr isochrons of selected leachate–residue–untreated clay fractions for illite samples from GMI Ridge.

Figure 10

Figure 10. ^{40}Ar–^{39}Ar step-heating for vacuum-encapsulated, sediment-hosted illite of < 0.5 μm (A & B), where f_{recoil} refers to the fraction of ^{39}Ar lost during recoil.

Figure 11

Figure 11. Close-up of sample area showing Cretaceous ages are only found in the Nappamerri Trough while Carboniferous and Triassic ages are restricted to the Gidgealpa (GR), Merrimelia (MR), Yanpurra (YR) and Innamincka (IR) ridge system.

Figure 12

Figure 12. Chronological chart showing consistency of Sm–Nd, Rb–Sr and Ar–Ar dating with rifting of the southern and eastern margins of Australia and opening of the Tasman Sea. All ages are plotted with 2σ error. The numbers refer to previously reported events as follows: (1) initiation of rifting along the southern margin (Bryan et al., 2012), (2) accelerated rifting and exhumation of the eastern margin (O'Sullivan et al., 1995), (3) opening of the Tasman Sea (Veevers et al., 1991), (4) emplacement of the Whitsunday silicic large igneous province (Bryan et al., 2012), (5) rifting of the southern margin of Australia (Williamson et al., 1990) and (6) break-up of the southern continental margin (Veevers, 1986).

Figure 13

Figure 13. Chronological chart showing consistency of Rb–Sr with emplacement of the BLS granite (1), Early Permian Eastern Australian Rift System (2), the Nappamerri Unconformity (3) and Late Triassic extension of eastern Queensland (4; Gatehouse et al., 1995; Allen et al., 1998; Mavromatidis, 2008; Korsch et al., 2009).

Figure 1

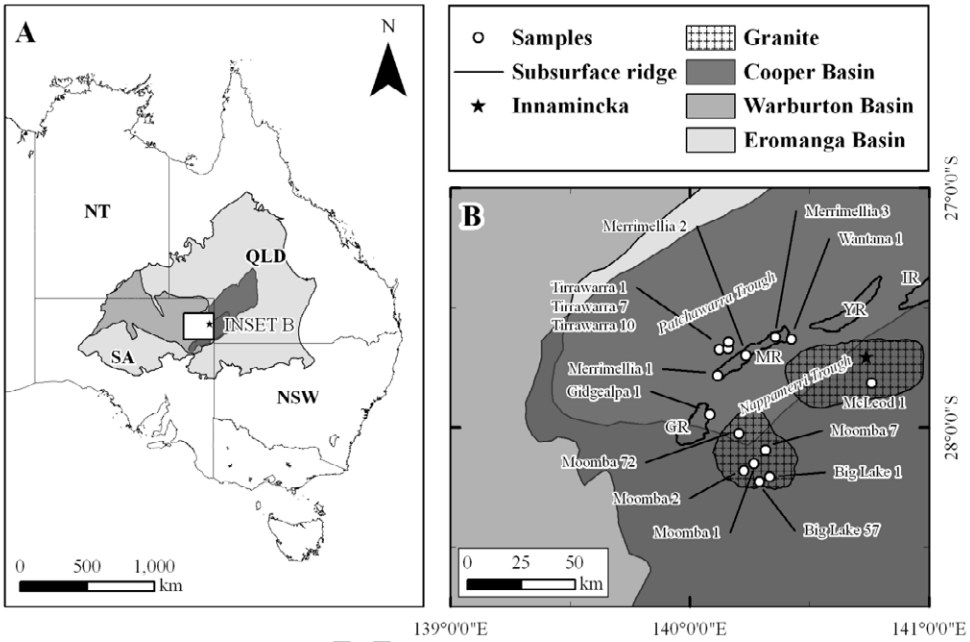

Figure 2

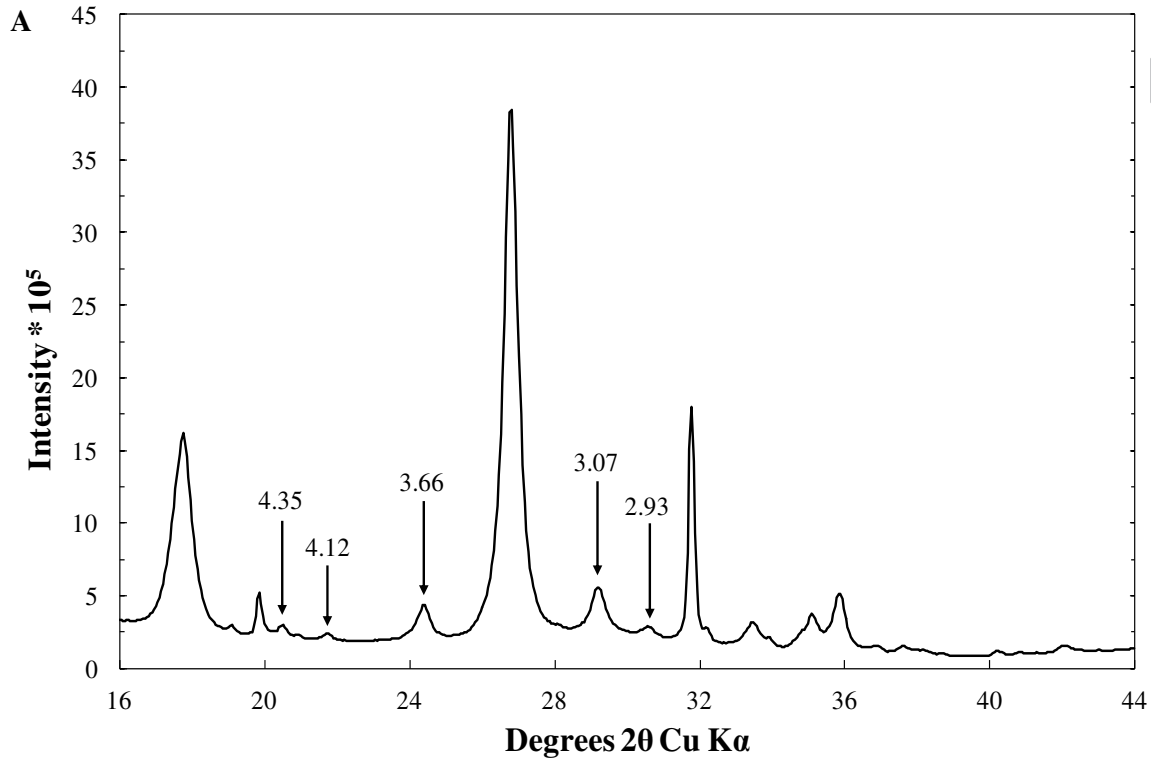

Figure 3

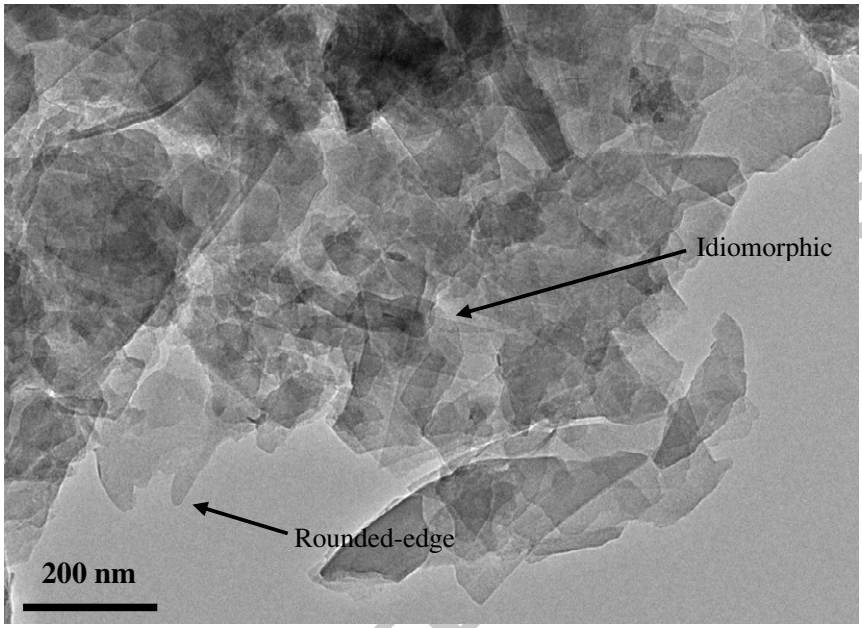

Figure 4

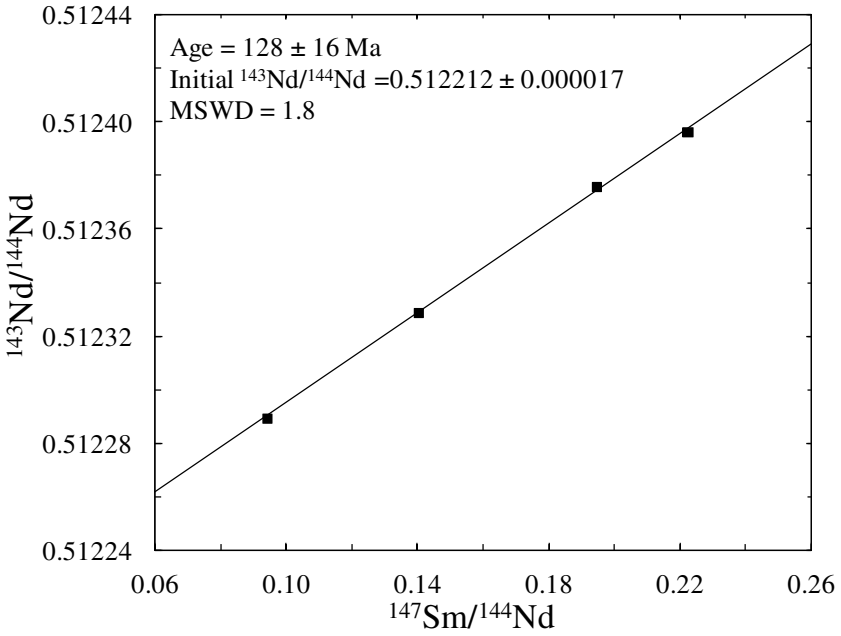

Figure 5

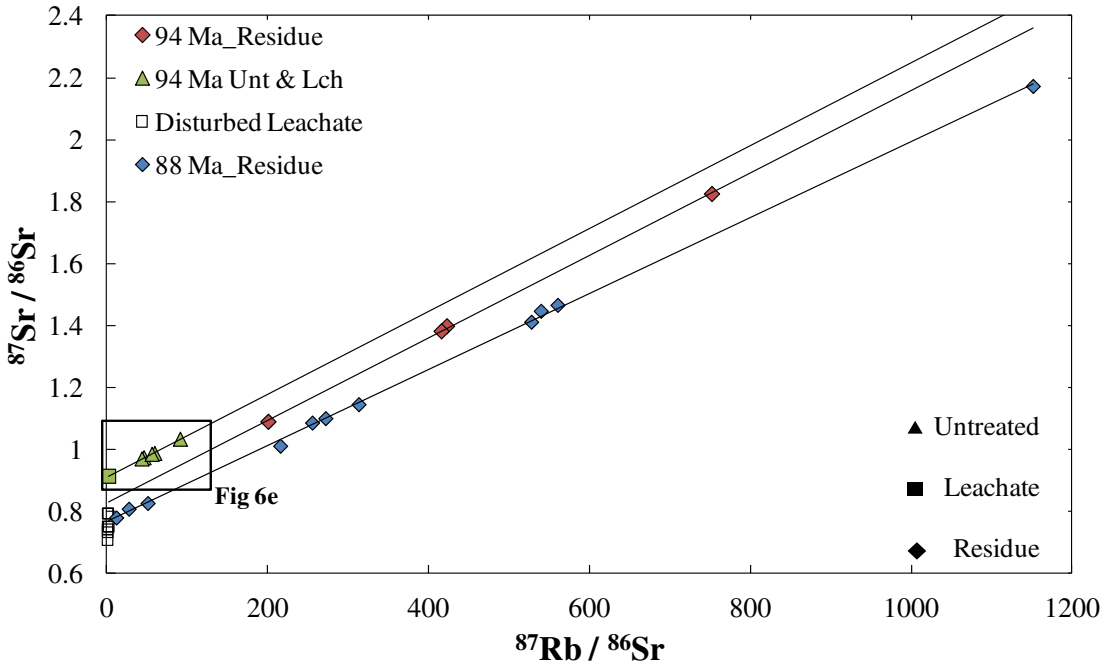

Figure 6

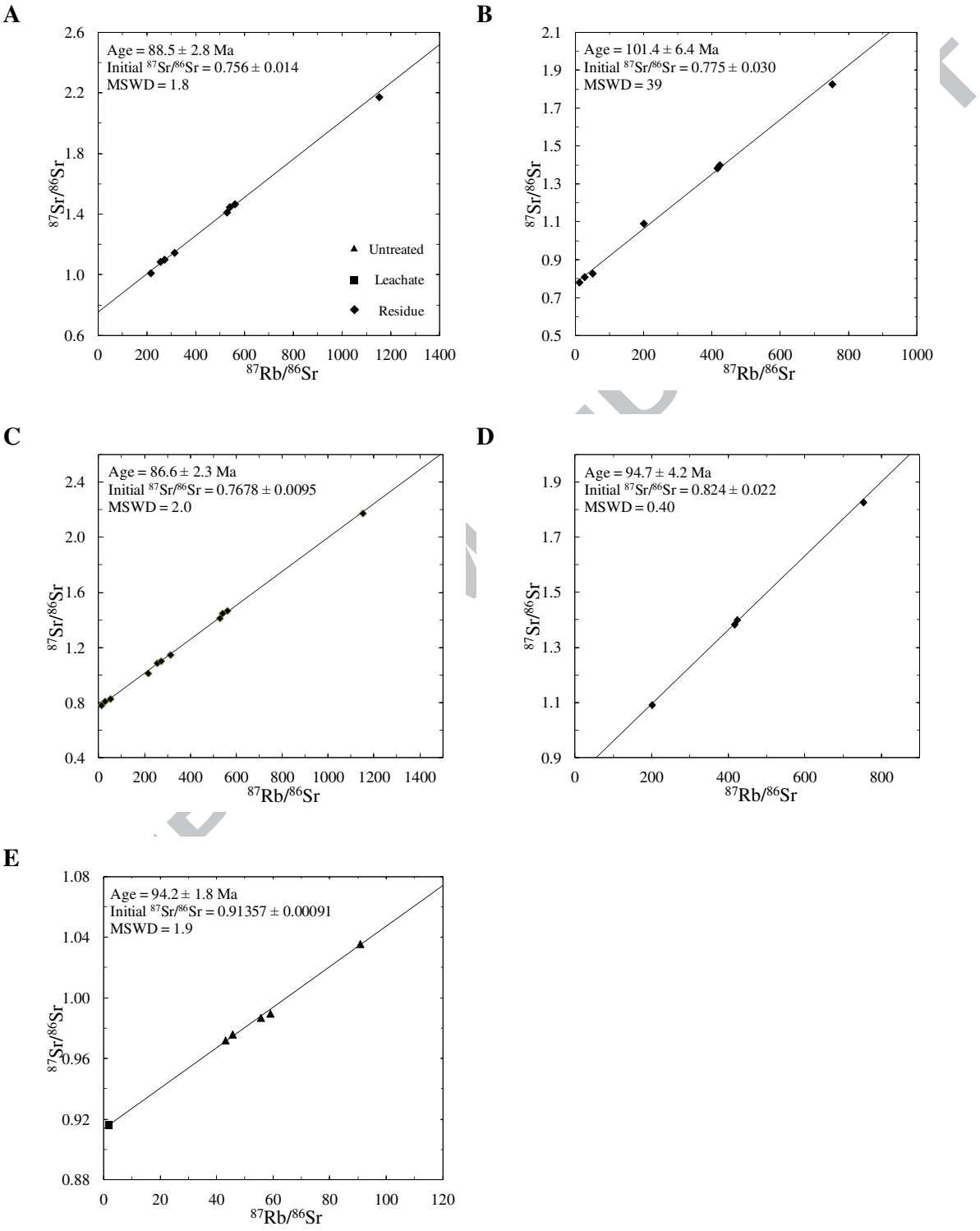

Figure 7

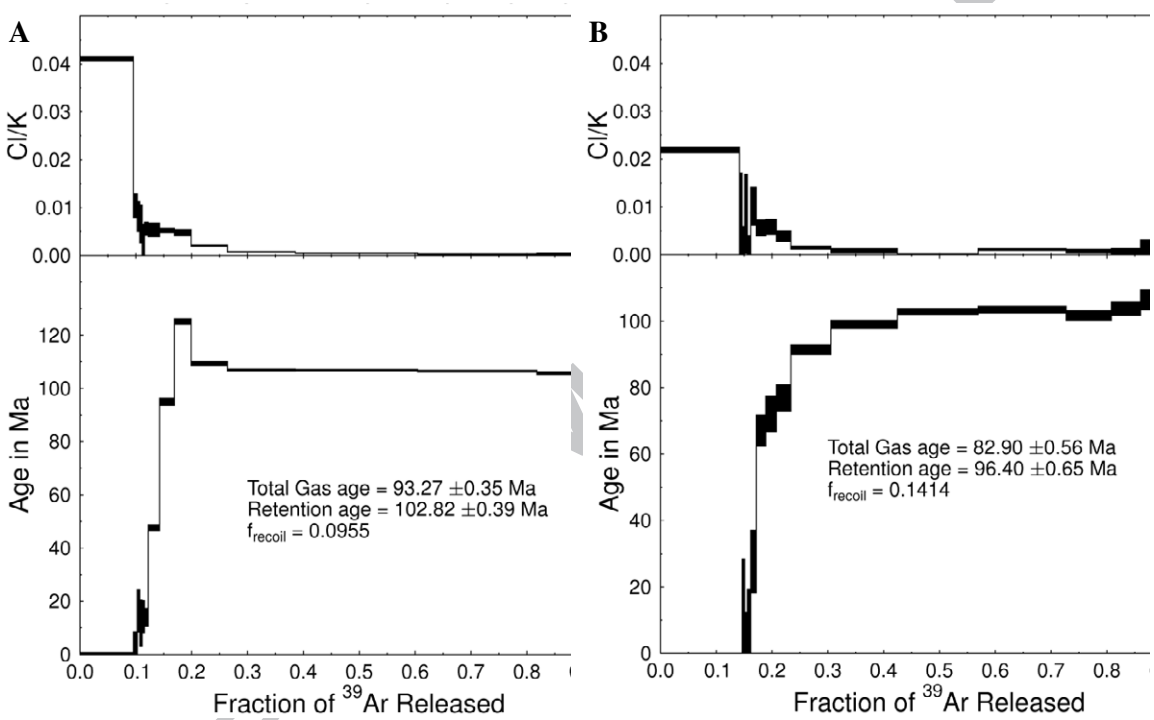

Figure 8

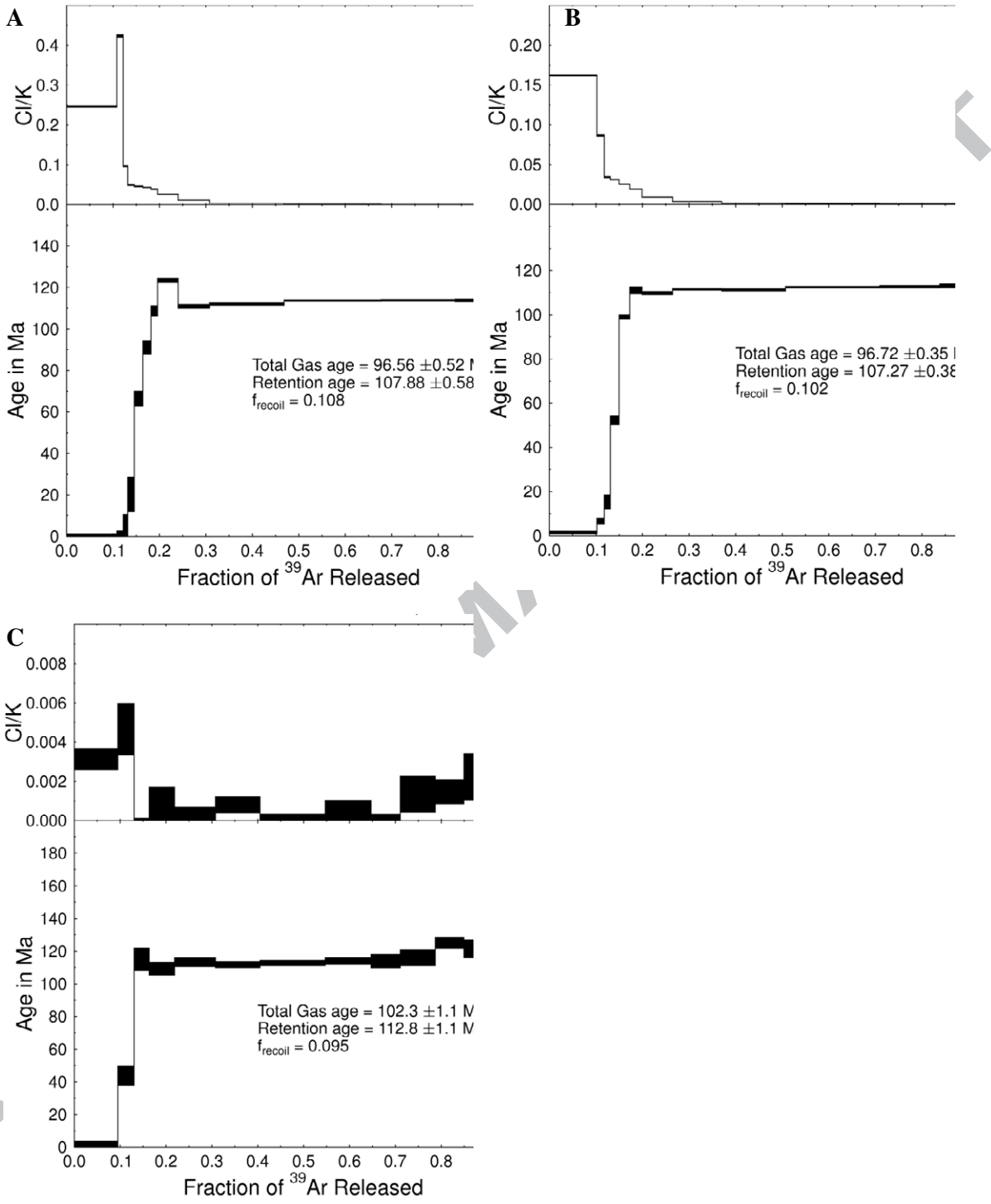

Figure 9

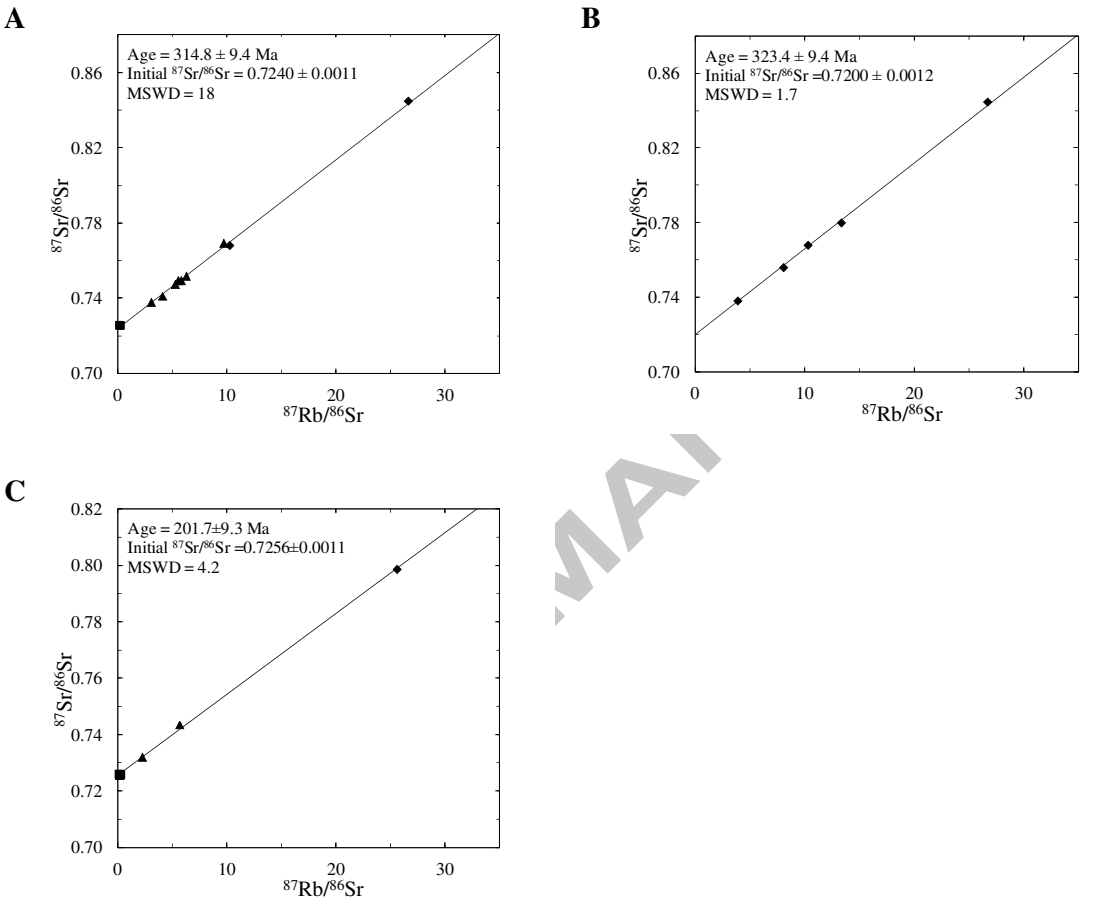

Figure 10

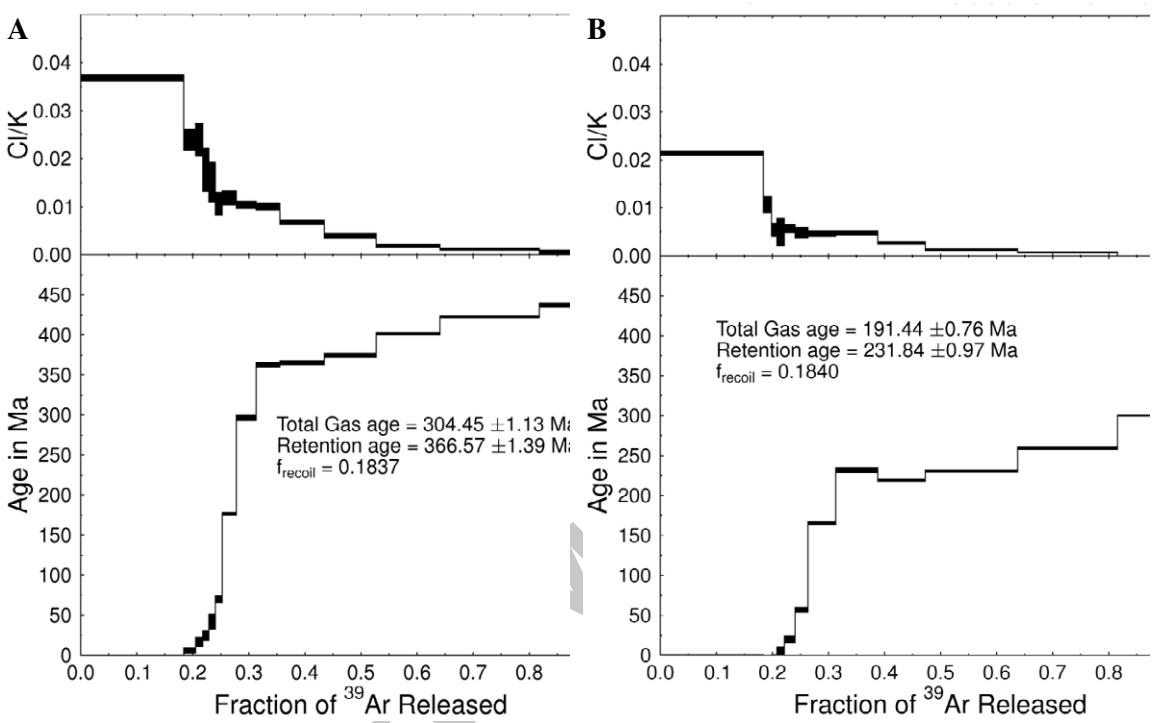

Figure 11

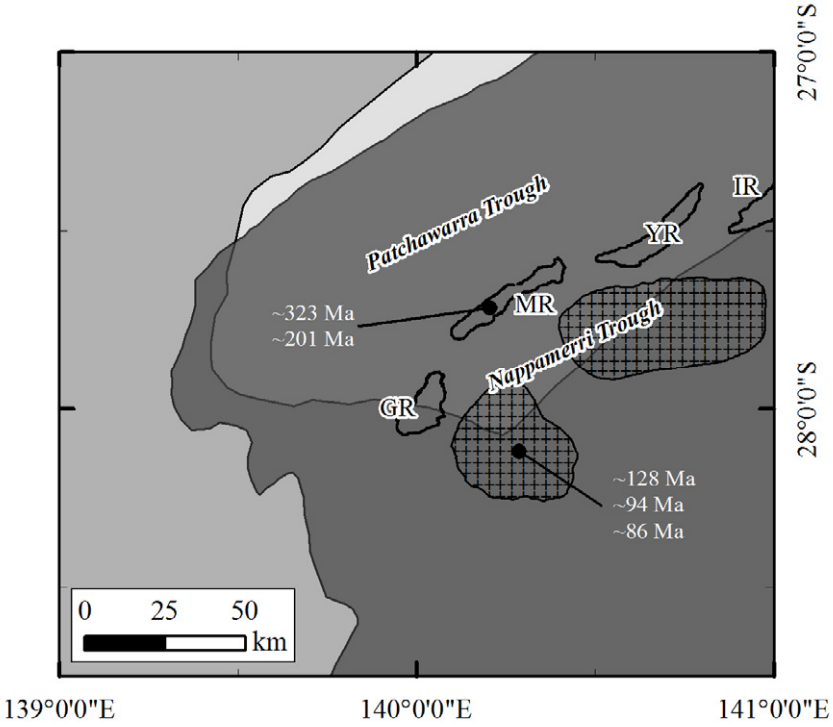

Figure 12

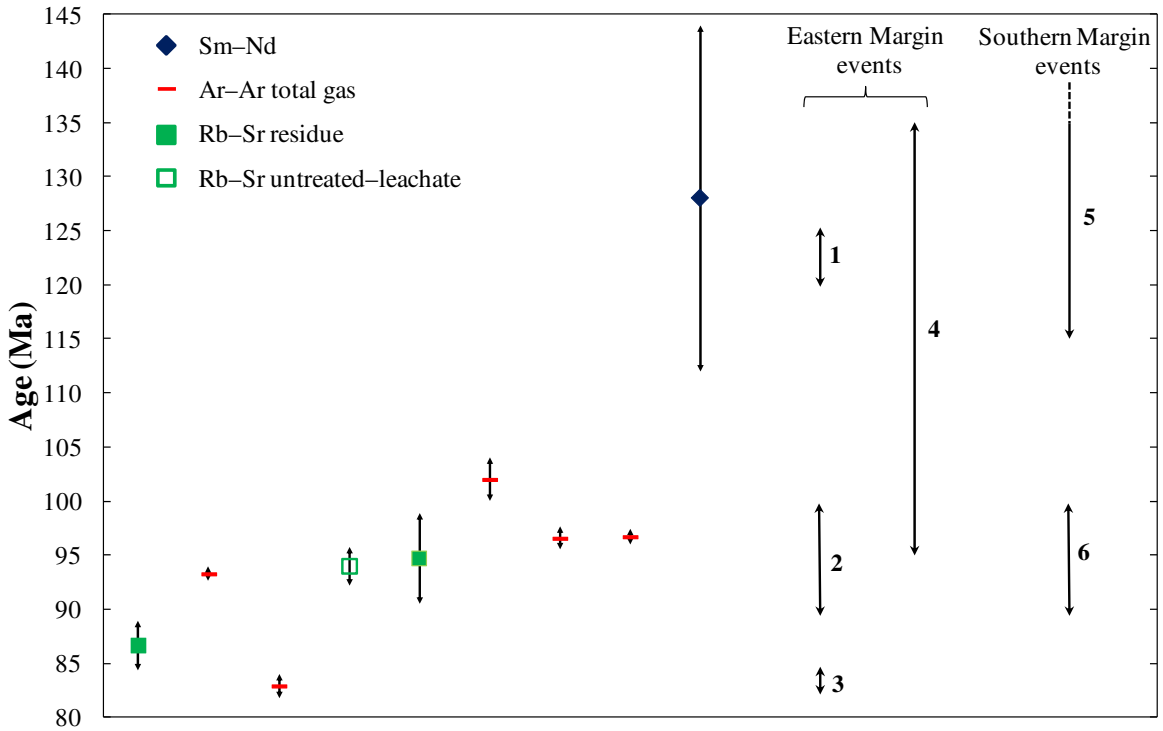

Figure 13

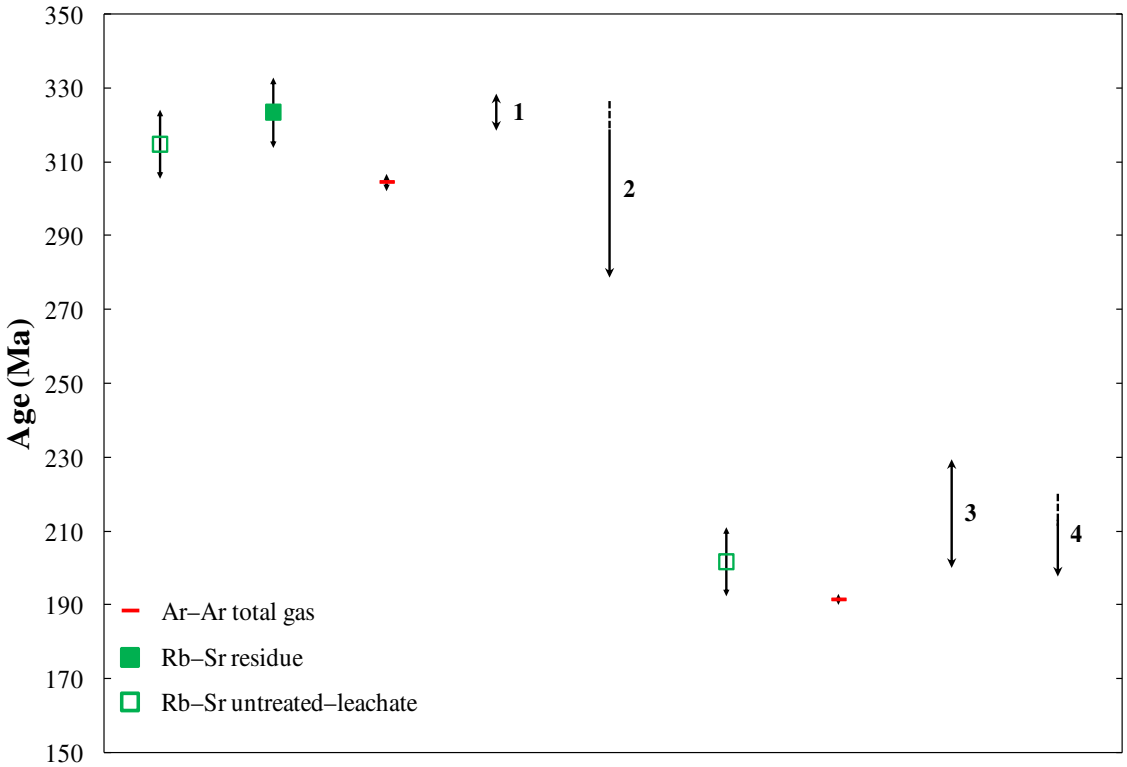

Table 1
^{147}Sm–^{144}Nd isotope data for illites from the Warburton–Cooper Basin

Sample	Grain Size (μm)	Aliquot	$^{147}Sm/^{144}Nd$	2σ	$^{143}Nd/^{144}Nd$	2σ	εNd (128 Ma)	εNd (present)
MB72_3008	2-1	U	0.0928	0.0007	0.512287	0.000010	-5.15	-6.85
MB72_2999.6	<2	U	0.1391	0.0011	0.512329	0.000008	-5.09	-6.03
MB72_3005	<2	U	0.1937	0.0047	0.512381	0.000018	-4.97	-5.01
MB72_3003.2	<2	U	0.2220	0.0015	0.512391	0.000010	-5.23	-4.82

U = untreated, L = leachate, R = residue.

Table 2

^{87}Rb–^{86}Sr data for the untreated, leachates, and acid-leached (residues) clay fractions from the Nappamerri Trough

Sample	Grain Size (μm)	Aliquot	Rb (ppm)	Sr (ppm)	$^{87}Rb/^{86}Sr$	$^{87}Sr/^{86}Sr \pm 2\sigma$
BL57_1748.94	2–0.5	L	7.400	67.76	0.091	0.710262 ± 9
MB7_2453.4	< 0.5	R	712.0	77.06	27.00	0.809948 ± 7
MB7_2453.3	< 2	R	381.8	97.59	11.39	0.781600 ± 9
MB7_2453.3	< 2	L	2.440	4.433	1.604	0.753191 ± 12
MB2_2715.5	< 1	L	7.128	129.7	0.162	0.745361 ± 9
MB1_2847.75	2–0.5	R	757.8	8.947	255.0	1.087784 ± 7
MB1_2847.75	< 0.5	R	553.1	3.243	527.4	1.413101 ± 11
MB1_2847.75	< 0.5	L	138.8	1114	0.363	0.795943 ± 8
MB1_2851	2–0.5	R	631.8	6.065	312.8	1.147164 ± 11
MB1_2851 a	< 0.5	R	670.5	3.744	539.3	1.448314 ± 23
MB1_2851 b	< 0.5	R	514.6	3.697	427.4	1.323200 ± 8
MB1_2857.4	2–0.5	R	625.5	8.655	215.3	1.012992 ± 8
MB1_2857.4	2–0.5	L	103.4	330.4	0.914	0.796436 ± 8
MB1_2857.4	< 0.5	R	573.2	3.181	560.1	1.467476 ± 12
MB1_2857.4	< 0.5	L	133.1	897.0	0.433	0.796103 ± 8
MB1 -2851.9	2–0.5	R	707.1	7.827	271.5	1.102066 ± 5
MB72_3003.2	< 2	U	731.1	46.41	45.57	0.976036 ± 10
MB72_2999.6	< 2	U	721.8	35.82	58.91	0.989821 ± 8

MB72_3008	<1	R	835.6	3.220	751.6	1.826862 ± 22
MB72_3008	2–1	R	962.3	6.818	415.4	1.383793 ± 11
MB72_3011.1	< 1	R	744.4	2.139	1151	2.173605 ± 17
MB72_3011.1	2-1	R	889.7	13.34	200.1	1.091834 ± 11
MB72_3011.1	2–1	L	642.2	993.7	1.908	0.916050 ± 9
MB72_3012	< 2	U	747.1	51.50	43.05	0.972083 ± 8
MB72_3012	2-1	R	1008	7.378	422.2	1.400096 ± 11
MB72_3012	2–1	U	678.4	36.29	55.55	0.987036 ± 8
BL1_3057.3	< 0.5	U	1967	64.73	90.70	1.035730 ± 10
McL1_3593.2	2–0.5	R	304.9	17.66	50.53	0.828317 ± 8
McL1_3593.2	2–0.5	L	200.3	1903	0.306	0.754681 ± 9
McL1_3749.1	2–0.5	L	288.0	1903	0.441	0.781319 ± 6
TIR10_3005.2	< 0.5	L	1.985	15.78	0.366	0.735706 ± 9

U = untreated, L = leachate, R = residue.

ACCEPTED MANUSCRIPT

Table 3

^{40}Ar–^{39}Ar ages of authigenic illite. All uncertainties are ±1σ

Sample	Grain Size (μm)	Total gas age (Ma)	"Retention age" (Ma)	% 39Ar recoil
MB1_2847.75	2–0.5	93.3 ± 0.4	102.8 ± 0.4	9.55
MB1_2857.4	2–0.5	82.9 ± 0.6	96.4 ± 0.7	14.14
MB72_3009.9	< 1	96.6 ± 0.5	107.9 ± 0.6	10.80
MB72_3012.0	< 1	96.7 ± 0.4	107.3 ± 0.4	10.20
MB72_3011.1	2–1	102.3 ± 1.1	112.8 ± 1.1	9.50
Mer1_3039.5	< 0.5	191.4 ± 0.8	231.8 ± 1.0	18.40
Mer1_3144.5	< 0.5	304.5 ± 1.1	366.6 ± 1.4	18.50

Table 4
^{87}Rb–^{87}Sr data for the untreated, leachates, and acid-leached (residues) clay fractions from the GMI Ridge

Sample	Grain Size (μm)	Aliquot	Rb (ppm)	Sr (ppm)	$^{87}Rb/^{86}Sr$	$^{87}Sr/^{86}Sr \pm 2\sigma$
Mer2_2541.7	<0.5	R	397.3	114.6	10.29	0.768026 ± 11
Mer2_2541.7	<0.5	U	352.1	182.8	5.585	0.749338 ± 18
Mer3_2589.2	<0.5	R	394.7	316.7	3.884	0.738213 ± 7
Mer2_2617.35	<0.5	R	390.8	84.82	13.33	0.780024 ± 11
Mer2_2617.35	<0.5	L	6.239	121.3	0.153	0.725609 ± 10
Mer2_2617.35	<0.5	U	372.6	184.8	5.840	0.749325 ± 7
Mer2_2617.35	1-0.5	U	420.8	389.1	3.132	0.737661 ± 9
Mer2_2653.5	<0.5	R	450.7	161.8	7.989	0.756067 ± 9
Mer2_2653.4	<0.5	L	10.68	131.4	0.240	0.725777 ± 9
Mer2_2653.4	<0.5	U	242.5	132.7	5.293	0.747149 ± 9
Mer2_2653.4	1-0.5	U	498.7	635.9	2.271	0.732002 ± 9
Mer1_3039.5	< 1	R	337.0	38.04	25.62	0.798586 ± 8
Mer1_3039.5	1-0.5	U	354.1	162.6	6.305	0.751630 ± 8
Mer1_3039.5	2-1	U	489.9	340.6	4.167	0.741026 ± 7
Mer1_3144.5	<0.5	U	333.0	99.22	9.741	0.769226 ± 9
Gil1_3843.5	<2	U	122.9	62.24	5.711	0.743495 ± 7
Mer2_3895	<0.5	R	376.7	41.98	26.67	0.844729 ± 10
Mer2_3895	<0.5	L	6.736	207.0	0.100	0.725989 ± 10

U = untreated, L = leachate, R = residue.

ACCEPTED MANUSCRIPT